

Semiannual Progress Report, Jan.-June, 1980

(NASA-TM-81103) STUDY OF BOUNDARY-LAYER
TRANSITION USING TRANSONIC-CONE PRESTON TUBE
DATA Semiannual Progress Report, Jan. -
Jun. 1980 (Oklahoma State Univ.,
Stillwater.) 99 p HC A05/MF A01

N80-28305

CSCL 01A G3/02

Unclassified
28139**STUDY OF BOUNDARY-LAYER TRANSITION****USING TRANSONIC-CONE PRESTON TUBE DATA**

Research Grant Number NSG-2396

Principal Investigators

T. D. Reed and P. M. Moretti



School of Mechanical and Aerospace Engineering
Oklahoma State University
Stillwater, Oklahoma 74078

The NASA Technical Officer for this Grant is:

F. W. Steintle, Jr.
Experimental Investigations Branch, 227-5
NASA Ames Research Center
Moffet Field, California 94035

Semiannual Progress Report, Jan.-June, 1980

STUDY OF BOUNDARY-LAYER TRANSITION
USING TRANSONIC-CONE PRESTON TUBE DATA
Research Grant Number NSF-2396

Principal Investigators

T. D. Reed and P. M. Moretti

School of Mechanical and Aerospace Engineering
Oklahoma State University
Stillwater, Oklahoma 74078

The NASA Technical Officer for this Grant is:

F. W. Steinle, Jr.
Experimental Investigations Branch, 227-5
NASA Ames Research Center
Moffet Field, California 94035

ACCOMPLISHMENTS

- I. An oral presentation was made on July 23 to Mr. F. W. Steinle and personnel of the Experimental Investigations Branch, NASA Ames. At that time, a review of technical progress was given.
- II. As discussed in detail within the accompanying report, a correlation of Preston-tube data with theoretical skin-friction coefficient has been achieved for the subsonic, compressible laminar boundary layers on the AEDC Cone. The recommended correlation has been developed using data from nineteen different wind-tunnel conditions and has an rms error in skin-friction coefficient of less than 5%.
- III. The STAN-5 computer program for boundary layer calculations is not sensitive to changes in cone pitch or yaw angles. Thus, if the effect of such angles on the correlation is to be studied, a more sophisticated analysis of three-dimensional, viscous flow will be needed, e.g., McRae, et al. [Ref. 1].
- IV. The simplified model for calculating the magnitude of Preston-tube pressures (as a function of boundary-layer profile, local static pressure, and probe geometry and position with respect to the wall) does not appear to be a fruitful approach. Thus a more rigorous analysis will be necessary if this type of sensitivity study is to be physically meaningful.
- V. An approach for developing a correlation for the subsonic, turbulent boundary layer and transitional region has been selected. Skin friction and velocity profiles, at the beginning of the turbulent boundary layer, can be estimated by using the correlation of Allen [Ref. 2] in conjunction with the Preston-tube data and the Wu and Lock and STAN-5 computer programs. Once the distribution of turbulent skin-friction and boundary layer profiles are available, a correlation between Preston-tube data and theoretical skin friction can be developed using the same techniques employed for the laminar boundary layer. Skin friction within the transition zone can be easily approximated by employing the empirical

intermittency function of Dharwan and Narasimha [Ref. 3]. Although this intermittency function is based on flat-plate measurements, the use of actual Preston-tube measurements to specify the extent of the transition zone will result in a very good approximation for the distribution of C_f through the transition zone.

- VI. In the case of laminar boundary layers, there is no need to employ the more sophisticated program of Wilcox and Rubesin. However, this program may still be useful in checking the STAN-5 results for compressible, non-adiabatic turbulent boundary layers. This analysis and option will be relegated to future work.
- VII. The supersonic wind-tunnel data cannot be successfully analyzed without a calibration of P_{ref} as a function of Preston-tube position, M_∞ and Re_{ft} . The corresponding calibrations for the flight experiments could conceivably be utilized, but this analysis will also be relegated to future work.

REMAINING TASKS TO BE ACCOMPLISHED
UNDER THIS GRANT

- I. The effects of changes in nose bluntness on pressure distribution along the AEDC cone will be investigated.
- II. Subsonic Preston-tube data will be used to study and compare the onset and extent of boundary layer transition for the corresponding flight and wind-tunnel flow conditions.
- III. Use the flight data to develop a correlation for subsonic laminar boundary layers, with and without heat transfer, and compare the results with the corresponding correlation of the wind-tunnel data. The pressure distribution, measured during flight, will be used to calculate the flow, rather than the theoretical pressures of Wu and Lock.

REFERENCES

1. McRae, D. S., Peake, D. J., and Fisher, D. F.: "A Computational and Experimental Study of High Reynolds Number Viscous/Inviscid Interaction About a Cone at High Angle of Attack," AIAA Paper No. 80-1422, July, 1980.
2. Allen, J. M.: "Reevaluation of Compressible Flow Preston-Tube Calibrations," NASA TM X-3488, February, 1977.
3. Dharwan, S. and Narasimha, R.: "Some Properties of Boundary Layer Flow During Transition from Laminar to Turbulent Motion," JFM, Vol. 3, Pt. 4, 1958, pp. 418-436.
4. Higuchi, H. and Rubesin, M. W.: "Behavior of a Turbulent Boundary Layer Subjected to Sudden Transverse Strain," AIAA Journal, Vol. 17, No. 9, Sept. 1979.

CORRELATION OF THEORETICAL LAMINAR SKIN
FRICTION WITH PRESTON-TUBE
MEASUREMENTS ON A
SUBSONIC CONE

By

AYMAN SAID ABU-MOSTAFA

Bachelor of Science

Cairo University

Faculty of Engineering

Giza, Egypt

1970

Submitted to the Faculty of the
Graduate College of the
Oklahoma State University
in partial fulfillment of
the requirements for
the Degree of
MASTER OF SCIENCE
May 1980

ORIGINAL PAGE IS
OF POOR QUALITY

ABSTRACT

The laminar boundary layer on a 10-degree cone in a transonic wind tunnel is studied. The inviscid flow and boundary layer development are simulated by computer programs. The effects of pitch and yaw angles on the boundary layer are examined.

Preston-tube data, taken on the Arnold Engineering Development Center (AEDC) Boundary-Layer-Transition Cone in the NASA Ames 11-ft Transonic Wind Tunnel, has been used to develop a correlation which relates the measurements to theoretical values of laminar skin friction. The recommended correlation is based on a compressible form of the classical law-of-the-wall.

The computer codes successfully simulate the laminar boundary layer for near-zero pitch and yaw angles. However, in cases of significant pitch and/or yaw angles, the flow is three-dimensional and the boundary layer computer code used here cannot provide a satisfactory model.

The skin-friction correlation is thought to be valid for body geometries other than cones. It accounts for variable property and heat transfer effects. The rms deviation between theoretical skin-friction coefficients and the corresponding correlation values is < 5 %. Thus, as perhaps

might be expected, this is a better correlation for compressible laminar flows than has been reported for compressible, turbulent layers. The new correlation can be employed in transonic-wind-tunnel tests to relate Preston-tube surveys along models to distributions of laminar, skin-friction coefficient.

ACKNOWLEDGMENTS

I am most grateful to Dr. Peter M. Moretti, my principal adviser, for giving me the opportunity to work on this project and for his helpful suggestions and advice during the course of this study.

I am greatly indebted to Dr. Troy D. Reed for his continuous supervision and excellent guidance.

I would like also to thank Dr. Lynn R. Ebbesen and the staff of the University Computer Center for their help in the development of the computer programs.

This study was arranged through a NASA Ames University Consortium Interchange NCA2-OR535-701, the financial support of which is greatly acknowledged.

REPORT OF RESEARCH
IN AERONAUTICS

TABLE OF CONTENTS

Chapter	Page
I. INTRODUCTION	1
II. OBJECTIVES	3
III. EXPERIMENTAL DATA	6
3.1 General Background	6
3.2 Apparatus and Measurements	7
IV. CALCULATION PROCEDURE	13
V. EXTENDED WU AND LOCK COMPUTER PROGRAM	16
5.1 Introduction	16
5.2 The Original Program	16
5.3 Subroutine ANGLES	17
5.4 Subroutine DIST	17
5.5 Subroutine INITIA	18
5.6 Checking Wu and Lock Calculations	18
VI. STANS COMPUTER PROGRAM	21
VII. EFFECT OF FLOW ANGLES ON BOUNDARY-LAYER CALCULATIONS	24
VIII. CORRELATION OF SKIN FRICTION	28
8.1 Theoretical Background	28
8.2 Choice of the Function F	29
8.3 The Curve-Fitting Program	31
8.4 Results and Improvements	32
8.5 General Remarks	37
8.6 Prozorov Correlation	39
IX. CONCLUSIONS	41
X. SUPPLEMENTARY OBSERVATIONS	42
BIBLIOGRAPHY	44
APPENDIX A - AZIMUTH ANGLE CALCULATION	47

APPENDIX A - CALCULATION OF PRESTREAM PROPERTIES	50
APPENDIX C - CALCULATION OF INITIAL PROFILES	52
APPENDIX D - FUNCTIONAL DEPENDENCE OF THE EFFECTIVE CENTER OF THE PROBE .	55
APPENDIX E - RAW DATA USED FOR SKIN-FRICTION CORRELATION	57
APPENDIX F - LISTING OF THE EXTENDED WU AND LOCK PROGRAM WITH AN EXAMPLE RUN .	62

LIST OF TABLES

ORIGINAL PAGE IS
OF POOR QUALITY

Table	Page
I. Cases Studied	12
II. Sensitivity of STANS Computations to Changes in Flow Angles	27

LIST OF FIGURES

Figure	Page
1. Effect of initial Profile on Laminar Shear Stress Computation	5
2. Geometry of the Probe	10
3. AEDC Transition Cone and Instrumentation	11
4. Flow Chart for the Analysis	15
5. Calculated Pressure Coefficient on Cone Surface for Various Pitch Angles	20
6. Theoretical Effects of Flow Angles on Effective Pressure at Different Heights in the Boundary Layer	26
7. Deviation of Predicted Skin-Friction Coefficient by Egn. (8.15) from Theoretical Values	35
8. Data Collapse About Correlation (8.15)	36
9. Schematic of Flow Angles	48

NOMENCLATURE

c_f	Local skin-friction coefficient	
c_p	Specific heat at constant pressure, = 0.24 Btu/lbm°R for air	
C_p	Preston-tube pressure coefficient, = $(P_{Pt} - P_w) / (0.5 \rho_e U_e^2)$	
D	Characteristic dimension of the probe, in.	
D_{eq}	Equivalent circular diameter of the probe, in.	
f'	Blasius velocity ratio, = u/U_e	
G	Gain factor for the pressure transducer, psi/in.	
g_c	Conversion factor, = 32.174 lbm·ft/lbf·s	
h	Enthalpy, Btu/lbm	
H	Pressure head, in.	
J	Mechanical to thermal energy conversion factor, = 778.2 lbf·ft/Btu	
k	Non-dimensional normal distance, = $2y/D$	
L	Cone axial length, in.	
M	Mach number	
P	Pressure, psf	ORIGINAL PAGE IS OF POOR QUALITY
Pr	Prandtl number	
q	Dynamic pressure, psf	
r	Recovery factor, or radial distance, in.	
R	Gas constant, = 53.35 lbf·ft/lbm°R for air	
R_D	Reynolds number based on D and U_w , = $U_e D / V_w$	
Re_{ft}	Freestream unit Reynolds number, = U_∞ / V_∞	

Re_x	Length Reynolds number, $= U_e x / \nu_e$
Re_θ	Momentum-thickness Reynolds number, $= U_e \theta / \nu_w$
T	Temperature, °R
T'	Reference temperature, °R
u	Longitudinal velocity inside boundary layer, ft/s
u_{pt}	Mean velocity across probe face, ft/s
u^*	Shear velocity, $= \sqrt{\tau_w / \rho_w}$
u^+	Normalized velocity for wall-law, $= u/u^*$
U	Velocity outside boundary layer, ft/s
x	Distance along cone surface, ft
X	Body force per unit volume, lbf/ft
x^*	Dimensionless independent variable, Eqn. (8.13)
y	Distance normal to cone surface, ft
y^*	Dimensionless dependent variable, Eqn. (8.8b)
y^+	Wall Reynolds number, $= y u^* / \nu_w$

Subscripts

aw	adiabatic wall
B	Blasius solution
c	for cone flow
e	at edge of boundary layer
eff	effective
eq	equivalent
E	external or outer
I	internal or inner
Pt	Preston-tube
ref	reference
s	shorted

ORIGINAL PAGE IS
OF POOR QUALITY

t total
w at wall or cone surface
W for wedge flow
o wind-off
 ∞ freestream condition

Greek Letters

α Angle of attack, deg.
 $\bar{\alpha}$ Effective angle of attack, deg.
 β Yaw angle, deg., or pressure gradient parameter
 γ Ratio of specific heats, = 1.4 for air
 δ Cone semi-vertex angle, deg., or boundary layer thickness, ft
 δ^* Displacement thickness of boundary layer, ft
 Δ Deflection or increment
 ϵ Azimuth angle, deg.
 η Blasius non-dimensional normal distance, = $y \sqrt{U_e / 2 \times \nu'}$
 θ Momentum thickness of boundary layer, ft
 μ Molecular viscosity, lbf-s/ft
 ν Kinematic viscosity, ft^2/s
 ν' Kinematic viscosity evaluated at the reference temperature, ft^2/s
 ρ Density, lbm/ft
 τ Shear stress, psf
 ϕ Angle between cone axis and resolved yaw vector, deg.
 ψ Stream function, lbm/s
 ω Normalized stream function, Eqn.(6.1)

CHAPTER I

INTRODUCTION

The overall objective of this research is a better understanding of boundary layer transition, as reflected in the capability to relate transition on models in transonic wind tunnels to the corresponding free-flight conditions. The particular objective of the work reported herein is to develop a correlation which relates Preston-tube measurements within a laminar boundary layer on a cone to the corresponding theoretical values of skin friction.

Preston-tube measurements along the surface of a sharp 1.0-degree cone were obtained in the NASA Ames 11-Ft Transonic Wind Tunnel [1]. The minimum and maximum pressure locations, obtained during a survey along the length of the cone, were interpreted as the onset and end of transition, respectively.

The boundary layer on the slender cone was simulated via the STAN5 computer code [2] which is an extended version of Patankar and Spalding's boundary layer program [3]. The inviscid flow was calculated with Wu and Lock's computer program [4], and the results were used as boundary conditions along the outer edge of the boundary layer. Subroutines were added to this program so that arbitrary combina-

tions of pitch and yaw angles can be input, and the pressure distribution along the ray corresponding to the Preston-tube survey is always generated. In addition, a subroutine was added to the Wu and Lock program to calculate the initial profiles needed for STANS.

The cone is assumed to be stationary, smooth and sharp-nosed. The probe is assumed to be stable, in contact with the cone surface, and lie totally inside the boundary layer. The flow is assumed to be axi-symmetric, adiabatic, compressible and without body forces. The flow outside the boundary layer is assumed to be inviscid and is calculated based on the cone geometry, i.e., viscous interaction is ignored. The study was restricted to laminar boundary layers on the cone at subsonic speeds.

The effect on the inviscid flow of yaw and pitch angles less than the cone semi-vertex angle is easily calculated with the Wu and Lock program. However, the STANS program is a two-dimensional boundary layer code and was found to be relatively insensitive to changes in these angles.

A least-squares curve-fitting program [10] was used to arrive at a simple correlation between skin friction and Preston-tube measurements for the laminar, subsonic boundary layer.

CHAPTER II

OBJECTIVES

The first objective of this study was to calculate the best possible initial profiles, which are required to begin numerical boundary-layer calculations, so that boundary-layer predictions would be uniformly accurate. In an earlier study by Huprikar [5], it was found that different starting profiles resulted in differences in the computed shear stress near the tip of the cone. An example of this is shown in Figure 1.

The second objective was to extend the functions of Wu and Lock's program [4], which calculates the inviscid pressure distribution on sharp cones at transonic Mach numbers, so as to automate calculation of the pressure distribution along a ray corresponding to the Preston-tube survey for non-zero pitch (α) and yaw (β) angles. This information then provides the inviscid boundary conditions for calculation of the boundary layer with STANS. The third objective was to obtain a correlation for skin-friction coefficient or wall-shear stress in terms of the Preston-tube pressure measurements, so that the Preston tube can be used as a skin-friction measuring device.

ORIGINAL PAGE IS
OF POOR QUALITY

The present research focuses on the NASA Ames wind tunnel data taken within laminar boundary layers on the AEDC Transition Cone at subsonic speeds.

ORIGINAL PAGE IS
OF POOR QUALITY.

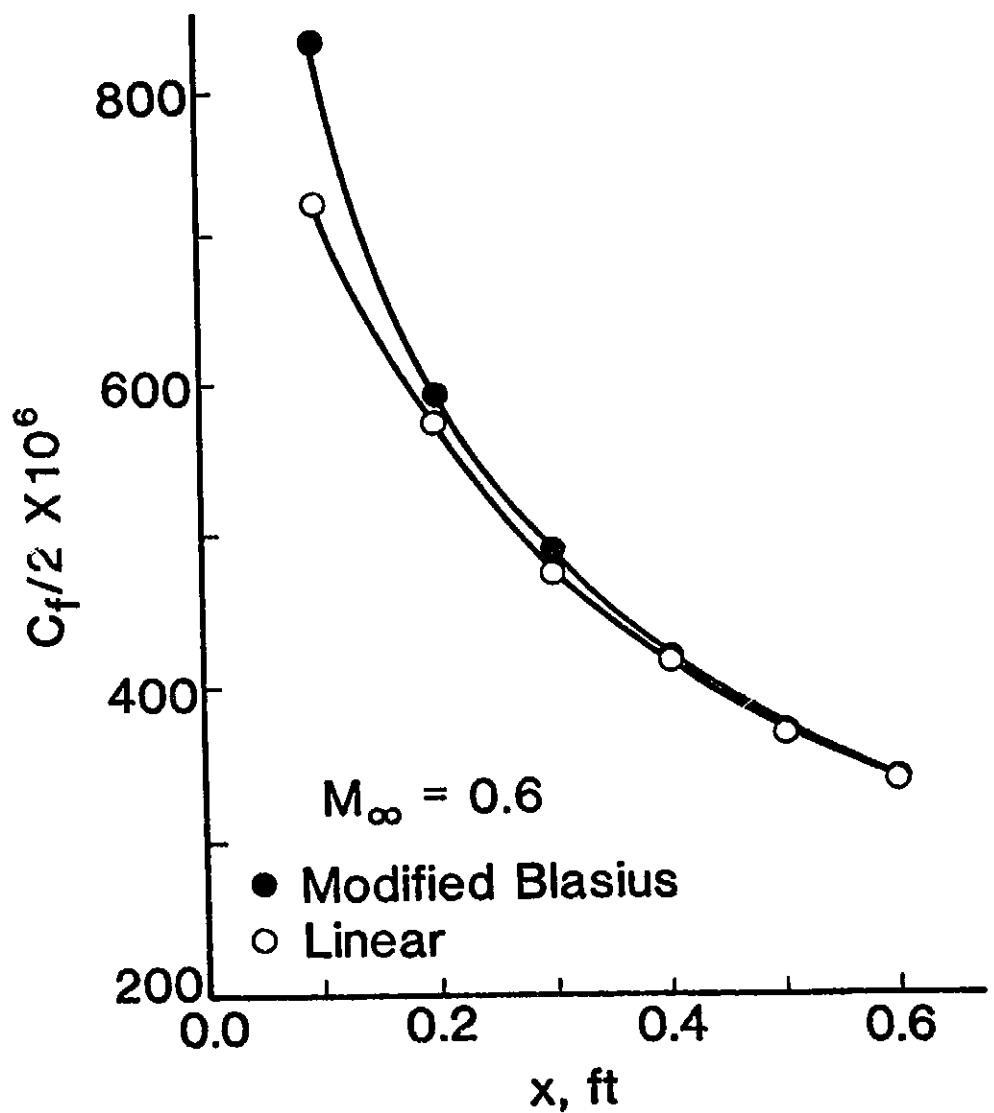


Figure 1. Effect of Initial Profile on Laminar Shear Stress Computation

CHAPTER III

EXPERIMENTAL DATA

3.1 General Background

The measurements utilized in this research were obtained in the NASA 11-Ft Transonic Wind Tunnel at Moffet Field, California. A transonic wind tunnel is an experimental facility intended to simulate the flow over scaled, aerodynamic-test models that would be similar to full-scale vehicles during free-flight through the atmosphere at Mach numbers from approximately 0.5 to 1.5.

In transonic flow the difference between the freestream velocity and the speed of sound is small compared to the magnitude of either, and the changes in these parameters are of comparable magnitude. This is contrasted to subsonic flow, where the velocity is lower than the sonic speed and where changes in Mach number are primarily due to changes in freestream velocity at essentially constant sonic speeds, and to supersonic flow where the magnitude of the freestream velocity is substantially larger than the local sonic speed with changes in Mach number occurring through variations of both parameters. In the transonic Mach number range, not only do compressibility effects become important, compared

to lower subsonic Mach numbers where the flow is incompressible, but also the flow at near-sonic speeds is complex because of the mixed type of flow which may exist with local supersonic flow fields contained in subsonic flow regions or local subsonic flow fields embedded in supersonic flow regions. That is why the cone shape is used as a model for boundary-layer-transition research; since it will not have local shocks along the conical surface. At high subsonic speeds, a shock may be generated near the base of the cone owing to flow expansion at the rear of the conical surface and a subsequent recompression in the wake. At supersonic speeds, the cone will, of course, also generate a bow shock, but a shock does not occur on the surface throughout the subsonic Mach number range.

It is worth mentioning that the ventilated, test-section walls of a transonic wind tunnel introduce acoustic and streamline disturbances into the test-section flow which means that the wind tunnel flow does not correspond exactly to transonic, free-flight conditions [6]. No satisfactory method has yet been derived to correct for all of the wall effects [7], although this is an area of active research [8].

3.2 Apparatus and Measurements

The experimental data were obtained from a Pitot probe that was traversed longitudinally along the surface of a 5-degree half-angle cone. The cross-section of the opening of the

probe is shown in Figure 2 193. The opening has an oval shape with the small dimension normal to the cone surface. The outer height of the probe face is 0.0097", while the centerline of the opening is 0.00453" above the cone surface. A schematic of the experimental model and instrumentation is shown in Figure 3.

The total pressure, as sensed by the Pitot probe, was measured by a differential pressure transducer. The reference pressure for the transducer was taken from the static holes on a flow-angularity probe mounted underneath the cone.

The output from the pressure transducer, ΔH , was recorded, during constant wind tunnel conditions, as a function of x on a plotter. Shorted output of the transducer, for the same wind tunnel conditions, was also plotted on the same plot. The output of the transducer, when the tunnel was off and the transducer was shorted, was also plotted. This output should theoretically be zero. This deflection is called 'wind-off' deflection.

Using this information, the total pressure P_{pt} , as measured by the Pitot probe can be deduced by using the relation

$$P_{pt} = P_{ref} + G(\Delta H + \Delta H_s + \Delta H_0) \quad (3.1)$$

Here P_{ref} is the reference static pressure which is considered to be equal to the freestream static pressure [9]. ΔH

is the deflection of the plotter corresponding to the magnitude of ΔP as sensed by the differential pressure transducer. The deflection from the shorted output is ΔH_S , and ΔH_0 is the wind-off deflection. G is the gain factor of the plotter, and its value is 0.2515 psi/in. This value was determined from the calibration of the plotter [5].

Twenty-one cases were chosen for detailed analysis. These are all the available, subsonic-wind-tunnel cases with near-zero flow angles. The tabulated data for these runs is shown in Table I. The freestream Mach number, unit Reynolds number and dynamic pressure are given by M_∞ , Re_{ft} and q_∞ , respectively, while α and β are the angles of attack and yaw, respectively.

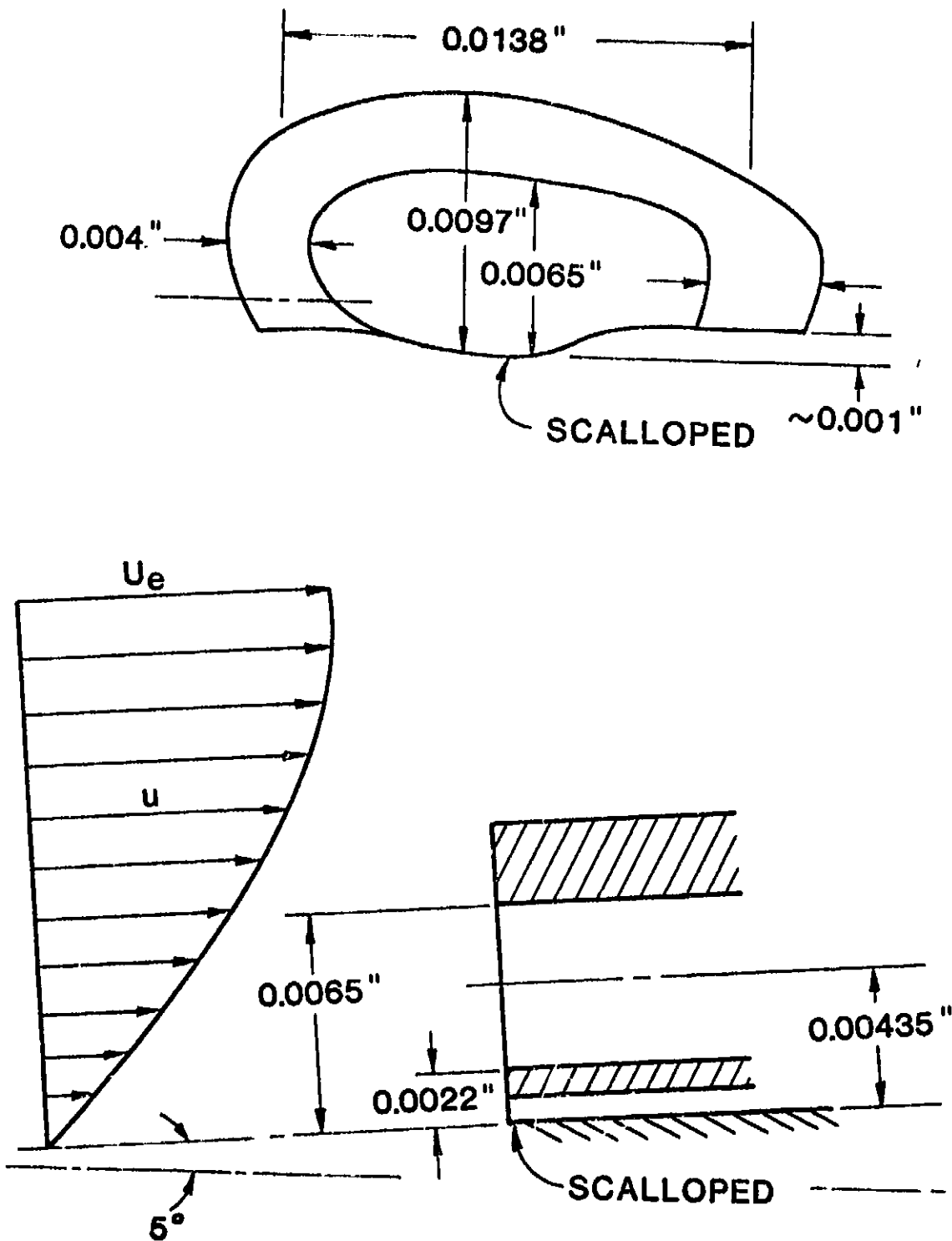


Figure 2. Geometry of the Probe

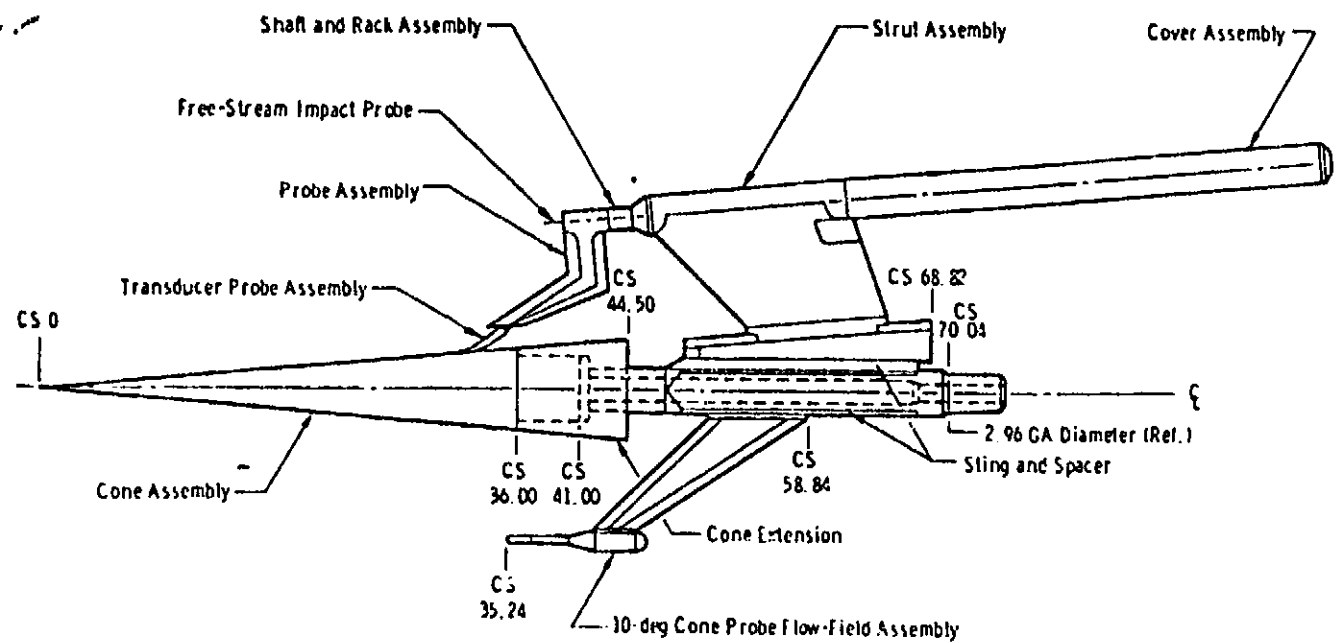


Figure 3. AEDC Transition Cone and Instrumentation

TABLE I
CASES STUDIED

<u>RUN NO.</u>	<u>M_∞</u>	<u>Re_{ft} x 10⁻⁶</u>	<u>q_∞</u>	<u>α°</u>	<u>β°</u>
15.231	0.95	4	693	-0.048	0.018
19.289	0.8	4	617	-0.003	-0.022
21.318	0.7	4	548	-0.006	-0.025
23.346	0.6	4	477	-0.001	-0.025
25.376	0.5	4	404	-0.005	-0.025
27.411	0.4	4	403	-0.004	-0.026
29.440	0.3	4	230	-0.006	-0.026
39.545	0.4	2.5	396	0.023	0.021
40.547	0.6	5	586	0.021	0.021
41.548	0.7	5	680	0.018	0.021
42.549	0.8	5	761	0.013	0.021
43.550	0.9	5	842	0.010	0.021
44.551	0.95	5	873	0.008	0.021
56.631	0.9	3	492	0.062	0.006
57.632	0.8	3	453	0.066	0.006
58.633	0.7	3	408	0.071	0.006
59.634	0.6	3	357	0.075	0.006
60.635	0.5	3	302	0.068	0.007
61.636	0.4	3	246	0.070	0.007
70.726	0.7	4	538	0.036	0.023
72.748	0.8	4	605	0.030	0.023

ORIGINAL PAGE IS
OF POOR QUALITY

CHAPTER IV

CALCULATION PROCEDURE

The calculation procedure consists of the following steps for each case studied :

1. The given freestream parameters (M_∞ , Re_{ft} , q_∞), as well as the flow angles (α , β), are fed into the extended Wu and Lock program. This program is described in the next chapter and is listed in Appendix F. The output is two-fold:

- a. The inviscid velocity distribution along the cone, and
- b. The initial profiles of velocity and stagnation enthalpy at a distance very close to the tip of the cone.

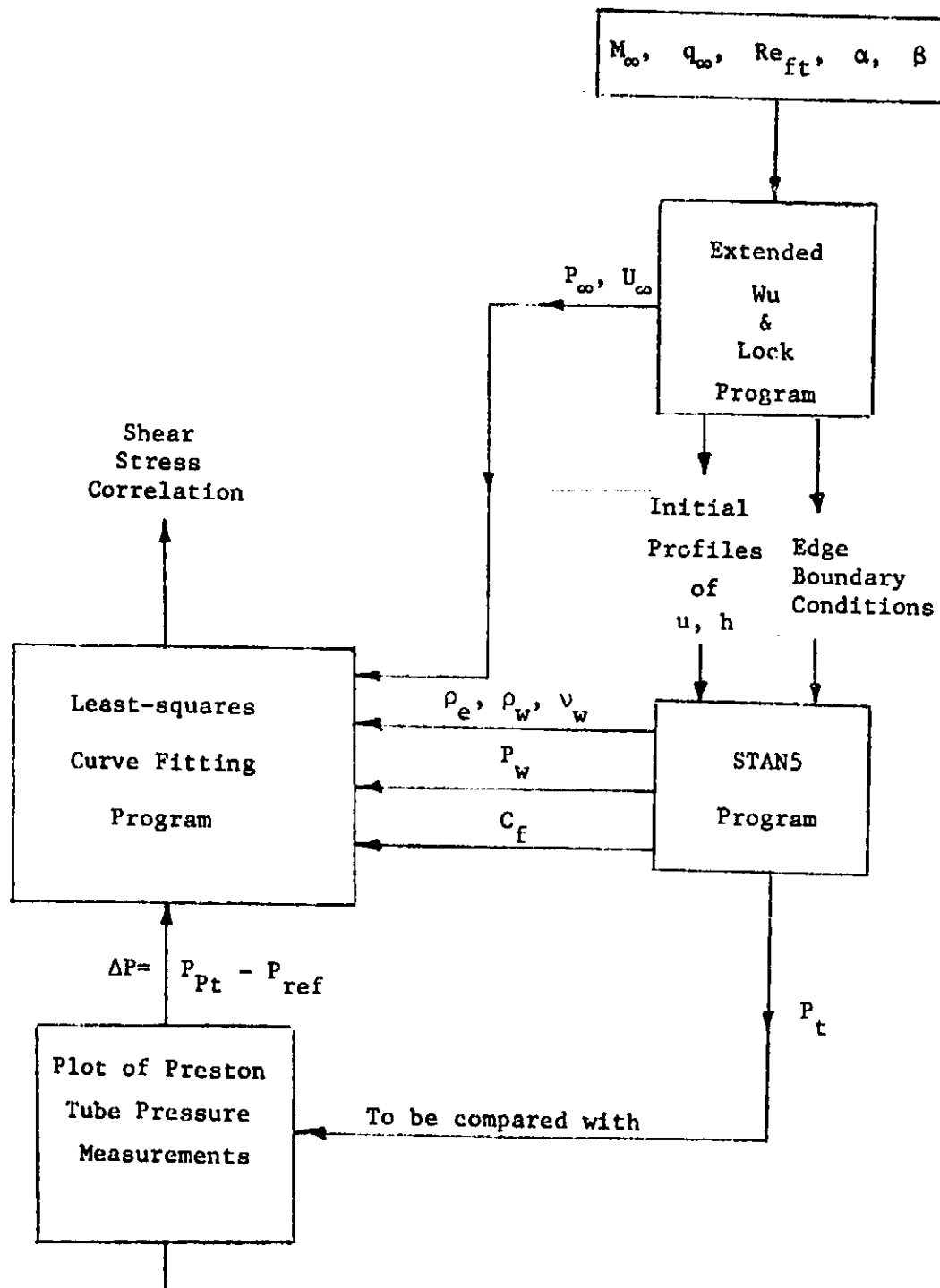
2. These results are then input to the STANS program. A brief description of STANS is presented in Chapter VI. The output from that program has detailed information on the boundary-layer properties along the ray of the cone which corresponds to the Preston-tube survey.

When correlation of skin friction was pursued, two more steps were followed :

3. Experimental Preston-tube pressure measurements were calculated from NASA/ANES 11 THT Preston-tube data [1] using Equation (3.1).

4. These experimental pressures, together with some other parameters* calculated by STANS, were fed into a curve-fitting program [10] to obtain the required correlation. Figure 4 is a flow chart that summarizes the calculation procedure described above.

*See Chapter VIII for details.



1. Effective center of probe
2. Effect of α , β
- ... etc.

Figure 4. Flow Chart for the Analysis

CHAPTER V

EXTENDED WU AND LOCK COMPUTER PROGRAM

5.1 Introduction

Wu and Lock [4] developed a computer program to calculate the inviscid transonic flow field over a sharp-edge smooth cone surface. The program appears to give accurate results [9] when compared with experimental observations. The program, however, handles only yaw angles less than the cone semi-vertex angle. The modified program presented herein calculates the following additional information :

1. The inviscid velocity and pressure distribution along a ray of the cone that corresponds to the Preston-tube survey for arbitrary combinations of α and β ,
2. The effect of yaw angles on the inviscid flow field, and
3. The velocity and total enthalpy profiles at a user-specified initial station.

The listing of the extended program can be found in Appendix F. Output for an example run (Case 25.376) is also included.

5.2 The Original Program

The main program reads in M_∞ , α , β , and the cone semi-vertex angle δ and calculates the inviscid-flow pressure

distribution along the cone surface. This is used as the pressure at the edge of the boundary layer. The theory and equations used are described in the Wu and Lock report [4]. The program prints out, along the cone length, the local Mach number M_e and the ratio P_w/P_∞ .

5.3 Subroutine ANGLES

This subprogram uses the angle-of-attack α and the yaw angle β to calculate the effective pitch angle $\bar{\alpha}$ and the azimuthal position of the probe ϵ . This subroutine utilizes the equations derived by Dunn et al [11]. These equations are presented in Appendix A. The probe position is considered to be always at the top of the cone and, in accordance with Wu and Lock's notation, $\epsilon = 0.0$ always corresponds to the leeward side of the cone. The calculated angles ($\bar{\alpha}$ and ϵ) are then used in the main program to calculate the inviscid pressure distribution along the top of the cone.

5.4 Subroutine DIST

This subroutine reads in the freestream dynamic pressure (QTINF), unit Reynolds number (REFT) and Mach number (MINF). It then uses these values to calculate the freestream properties (PINF, TINF, RHOINF, MUSINF) as well as the total temperature and pressure (TTOT, PTOT). The equations used are the equation of state for a perfect gas (air), Sutherland's equation of viscosity and the isentropic relations [12]. The

details of the calculations are described in Appendix B.

Next, the subroutine uses the local Mach numbers at stations along the cone surface, which are calculated in the main program, to calculate the local temperatures and velocities using isentropic relations. These velocities are then used as the outer boundary conditions for calculation of the boundary layer using STAN5.

5.5 Subroutine INITIA

This last subprogram calculates the velocity and stagnation enthalpy profiles across the boundary layer at a specified initial location. It calculates the average static temperature and viscosity across the boundary layer and uses them to modify the flat-plate Blasius solution so as to apply to the cone problem. The details are presented in Appendix C.

5.6 Checking Wu and Lock Calculations

As a check on the reliability of our version of Wu and Lock's program, the inviscid flow was calculated for a 10-degree cone at a 2-degree pitch angle and compared with those in Wu and Lock's report [4]. The following observations were made :

- a. Static pressures on the windward side of the cone are larger than those on the leeward side.
- b. Increasing α increases the static pressure on the windward side and decreases it on the leeward side.
- c. The slope of the pressure distribution is essentially

the same on both the windward and leeward sides of the cone.
(except near the tip and the rear ends of the cone). These
checks are shown in Figure 5.

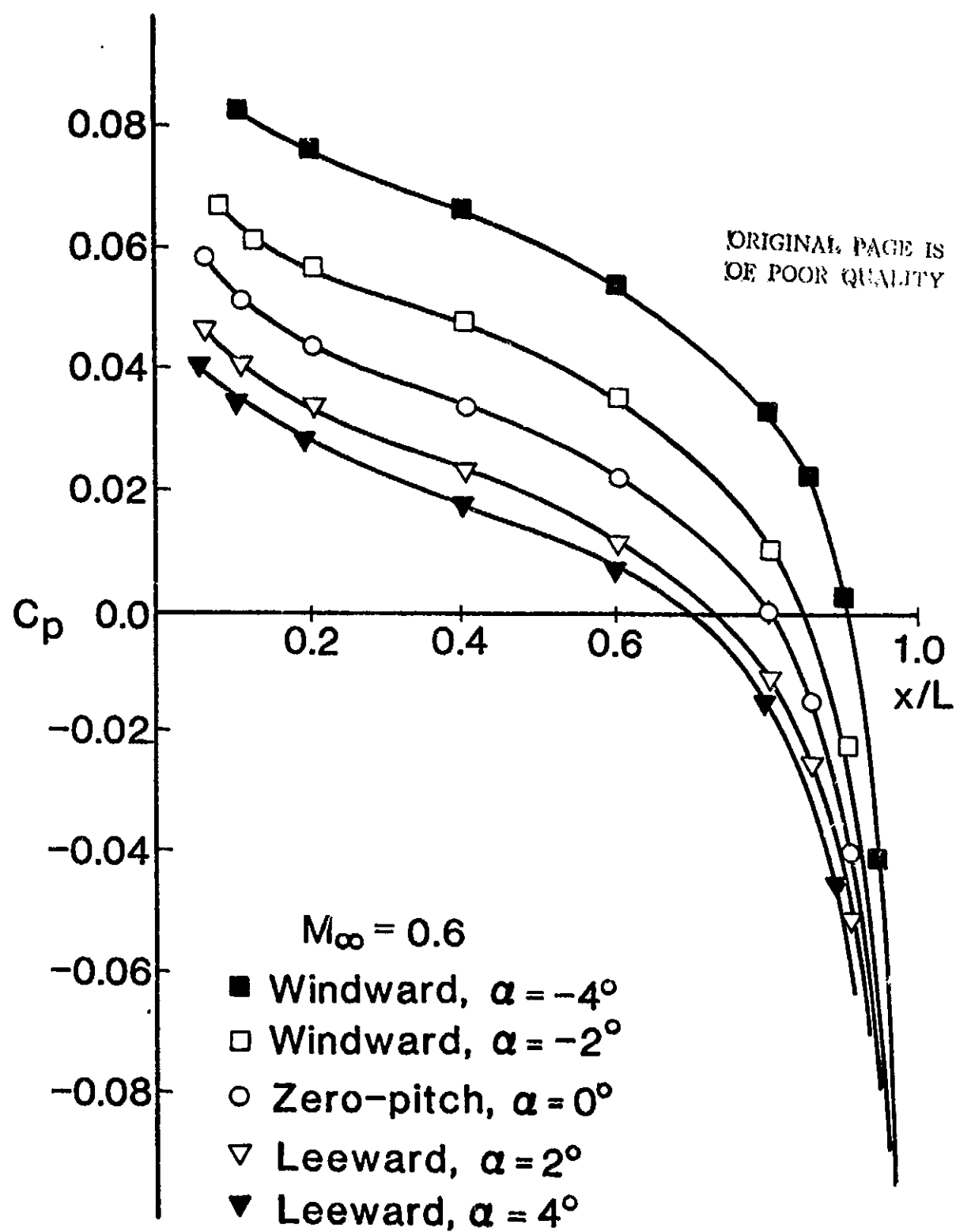


Figure 5. Calculated Pressure Coefficient on Cone Surface for Various Pitch Angles

CHAPTER VI

STANS COMPUTER PROGRAM

Based on the work of Patankar and Spalding [3], the STANS code was developed by Crawford and Kays [2] as an implicit, finite-difference, forward-marching integration procedure which may be used for computer simulation of boundary layers with transition. The program solves simultaneously equations for conservation of mass, momentum, stagnation enthalpy and up to five mass transfer equations.

The program uses either two-dimensional planar or axisymmetric type of coordinates so that it is possible to solve for a large variety of flows by simple manipulation of variables. This is accomplished by replacing the y -coordinate with the stream function ψ . The u -velocity component is defined by

$$u = \frac{1}{\rho r} \frac{\partial \psi}{\partial y}$$

and the momentum and energy equations become

$$\rho u \frac{\partial \psi}{\partial x} + \rho u \frac{\partial}{\partial \psi} \left[r^2 \rho u \mu_{eff} \frac{\partial u}{\partial \psi} \right] = -g_c \frac{dp}{dx} + g_c x,$$

and $\rho u \frac{\partial h_t}{\partial x} + u \frac{\partial}{\partial \psi} \left[r^2 \rho u \frac{\mu_{eff}}{Pr_{eff}} \frac{\partial h_t}{\partial \psi} \right]$

$$\frac{\partial}{\partial \psi} \left[\frac{\mu_{eff}}{g_c J} \left(1 - \frac{1}{Pr_{eff}} \right) r^2 \rho u \frac{\partial}{\partial \psi} \left(\frac{u^2}{2} \right) \right]$$

The stream function ψ is then normalized by using the transformation

$$\omega = \frac{\psi - \psi_I}{\psi_E - \psi_I} \quad (6.1)$$

where ψ_E and ψ_I are the stream function values on the boundary surfaces or boundary conditions.

A micro-integral method is used to obtain implicit finite-difference equations, which model the partial differential equations and may be used in a downstream, forward-marching solution scheme. The program solves laminar and turbulent boundary layers. Boundary-layer transition is based on the momentum-thickness Reynolds number criterion, which is defined a priori. The way the transition Reynolds number (RETRAN) is specified is as follows :

A very large value is assigned to RETRAN, e.g. 10000, so that the program is ensured to run wholly laminar. From the experimental data sheets obtained from NASA [1], the location of the minimum pressure is considered to be the onset of transition. At this location the corresponding value of Re_θ in STANS output is then considered to be the correct RETRAN.

However, since we are presently concentrating only on the laminar boundary layer, a large value of RETRAN was always assigned in the input to STANS and no re-run was necessary.

Other input parameters and "flags" are required, a detailed description of which can be found in the STANS report L2J. The edge velocity distribution and initial profiles for the velocity and total enthalpy across the boundary layer are required input for STANS. They are prepared by the extended Wu and Lock program. (See Chapter V).

The output of the program gives, at every incremental x , all the boundary-layer properties of interest, e.g., $u(y)$, $u^+(y)$, $y^+(y)$, C_f , δ , δ^* , θ , Re_θ , P_w , $T(y)$, $T_t(y)$, $P_t(y)$, ... etc. This information can then be used for theoretical analysis of the boundary layer.

CHAPTER VII

EFFECT OF FLOW ANGLES ON BOUNDARY-LAYER CALCULATIONS

As mentioned before in Chapter V, the angles of the free-stream flow will affect the boundary-layer flow.* One of the objectives of this research was to investigate the capability of the available computer programs (Wu and Lock's and STAN5) to handle pitch and yaw angles that are a significant fraction of π and to obtain some conclusions regarding the analytical tools needed to analyze such cases.

The original Wu and Lock program was modified to calculate the effective yaw angle for arbitrary combinations of yaw and pitch angles. The equations derived by Dunn et al [11] were used in subroutine ANGLES to calculate the azimuth angle of the probe, as discussed in Chapter V. It was found that the extended Wu and Lock program works well with all the cases studied.

One case was studied in some detail, viz., Case 40.547 which has the following data :

$$M_\infty = 0.6, Re_{ft} = 5 \times 10^6, q_\infty = 586 \text{ psi},$$

$$\alpha = \beta = 0.021^\circ.$$

*Transition is affected when α/δ is changed by $\pm 5\%$.
(Reference 9).

This case was picked up as a start because of its relatively small Mach number would allow neglection of noise effect [14],[15]. The output of the program (edge velocities and initial profiles) was input to STANS. It was found that the results of STANS for this case were exactly the same as the case of zero flow angles. This was not unexpected since (α) and (β) are very small in this case.

Then, the same case was repeated but with larger angles, viz., $\alpha=2.0$, $\beta=2.0$ degrees, which places the probe 135° from the windward element, and $\alpha=-2.0$, $\beta=2.0$ degrees which places the probe 45° from the windward element. The results of these two runs, together with the original run, are shown in Figure 6. k is defined as $2y/D$. The plotted results agree with the observation that the pressures on the windward side are greater than those on the leeward side and that a zero-incidence flow lies in between these. However, by comparing the values of wall shear stress, at the probe azimuth angle, and the boundary-layer thicknesses δ , δ^* , θ , the effect of α and β is negligible as show in table II. It was, therefore, decided to confine the present stage of research to the cases of very small flow angles. A possible reason for STANS's insensitivity is its assumption of axisymmetry while real flow with large pitch and/or yaw angles will have significant cross flow, thus forming a three-dimensional flow.

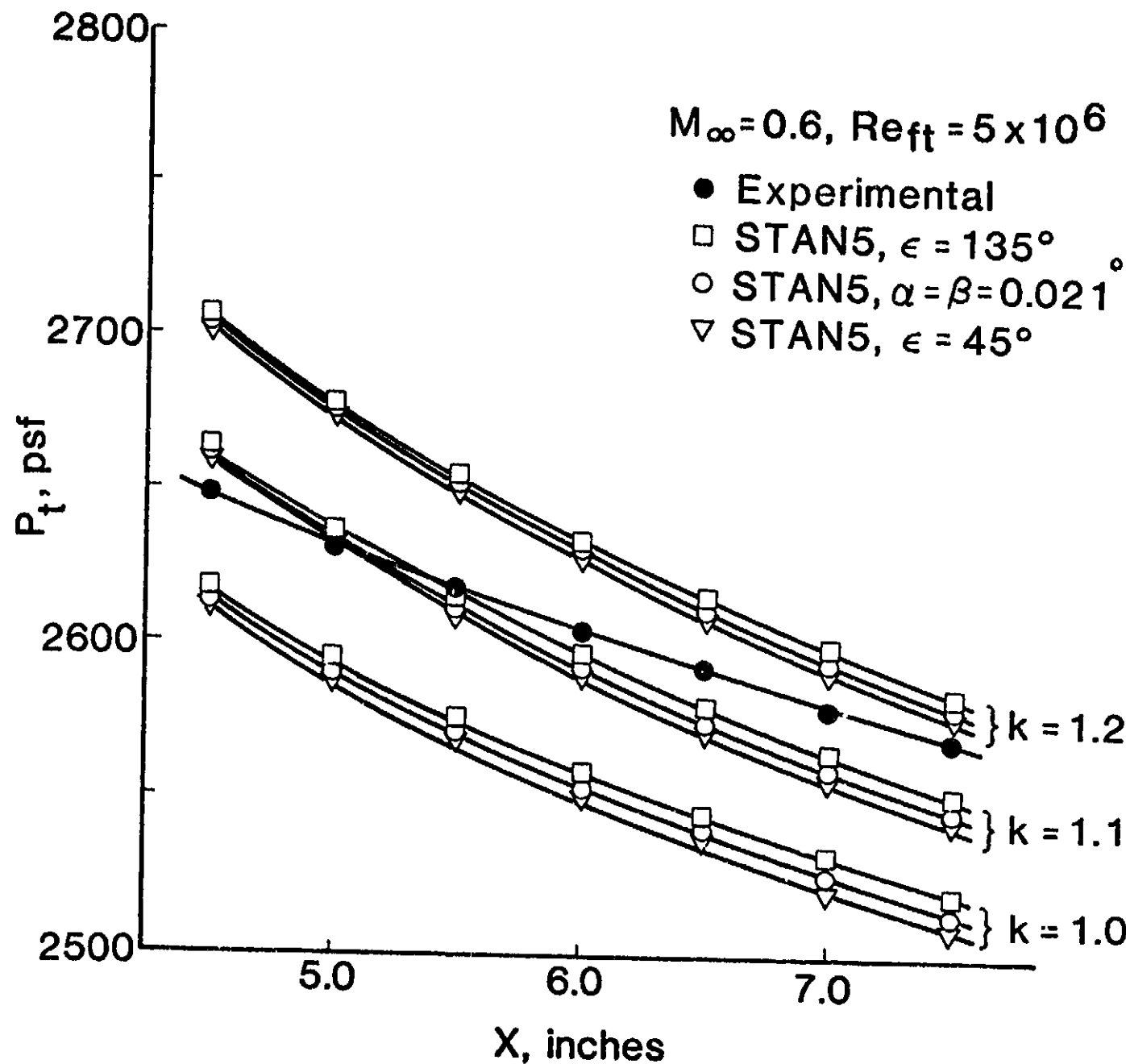


Figure 6. Theoretical Effects of Flow Angles on Effective Pressure at Different Heights in the Boundary Layer

TABLE II

SENSITIVITY OF STANS COMPUTATIONS TO
CHANGES IN FLOW ANGLES^a

x, ft	$\alpha = \beta = 0.021^\circ$				$\alpha = \beta = 2.0^\circ$ $\epsilon = 135^\circ$				$\alpha = -2.0^\circ, \beta = 2.0^\circ$ $\epsilon = 45^\circ$			
	$C_f/2$	δ	δ^*	θ	$C_f/2$	δ	δ^*	θ	$C_f/2$	δ	δ^*	θ
0.1	842	615	153	56	838	572	153	56	843	574	153	56
0.2	593	811	216	78	590	849	216	78	593	853	217	78
0.3	483	999	265	95	482	1020	264	95	484	1025	265	96
0.4	417	1157	305	110	417	1182	305	110	419	1188	306	110
0.5	374	1310	341	123	372	1322	341	122	375	1330	342	123
0.6	341	1449	374	134	340	1425	374	134	342	1430	374	134

^aAll numbers, except x, are multiplied by 10^6 . The case analyzed is 40.547. The azimuthal angle, ϵ , corresponds to the probe located at the top of the cone.

CHAPTER VIII

CORRELATION OF SKIN FRICTION

8.1 Theoretical Background

Dimensional analysis [17] has led to a wall-law of the form

$$u^+ = f(y^+) \quad (8.1)$$

where $u^+ = u/u^*$, $y^+ = u^*y/v$ and

u =longitudinal velocity, u^* =shear velocity $= \sqrt{\tau_w/\rho}$

If we use the incompressible Bernoulli equation to relate u to the pressure difference between a Preston tube resting on the wall and local static pressure, the law-of-the-wall can then be written in the following form.

$$u_{pt} = \sqrt{2(p_{pt} - p_w)/\rho} = \sqrt{2 \Delta P / \rho} \quad (8.2)$$

$$\frac{\sqrt{2 \Delta P / \rho}}{\sqrt{\tau_w / \rho}} = f\left(\frac{u^* y_{eff}}{v}\right) \quad (8.3)$$

Now, if we further assume that the effective center of the probe, y_{eff} , is at its half-height, i.e., $k_{eff} = 2y_{eff}/D = 1.0$, then

$$\frac{\Delta P}{\tau_w} = g\left(\frac{u^* D}{2v}\right) = g\left(\sqrt{\tau_w D^2 / 4\rho v^2}\right) \quad (8.4)$$

Now multiply the numerator and denominator on the left by the appropriate factor, in order to obtain the same grouping of terms as appear in the function g .

$$\frac{\Delta P D^2 / 4\rho v^2}{\tau_w D^2 / 4\rho P^2} = g\left(\sqrt{\tau_w D^2 / 4\rho v^2}\right)$$

or

$$\frac{\tau_w D^2}{4 \rho v^2} = F\left(\frac{\Delta P D^2}{4 \rho v^2}\right) \quad (8.5)$$

This last relation provides a convenient way for determining the skin friction since the shear stress is now uniquely related to the difference in pressure head measured with a Preston-tube static-hole combination. For a Preston tube of given geometry, the function F can theoretically be determined from pipe flow experiments where the skin friction can be deduced from measurements of pressure drop. In view of the fact that the wall-laws for pipe and boundary layer flows are identical [17], the calibration is expected to hold also in boundary layer flows.

Equation (8.5) is for incompressible flow in which the assumption of constant properties is valid. For our case, the flow is compressible and the properties, therefore, are not constant. For applications to Preston-tube data, the properties in Equation (8.5) should be evaluated at the wall (cone surface) [13], i.e.,

$$\frac{\tau_w D^2}{4 \rho_w v_w^2} = F\left(\frac{\Delta P D^2}{4 \rho_w v_w^2}\right) \quad (8.6)$$

The choice of wall properties is consistent with Bradshaw and Unsworth's correlation [20] for compressible, turbulent boundary layer.

8.2 Choice of the Function F

Patel [16], [17] established calibration curves for the laminar sublayer, buffer or transition region and

fully-turbulent layers. His correlation for the laminar sublayer is

$$y^* = 0.5 x^* + 0.037 \quad (8.7)$$

where x and y are defined, for compressible flow, as follows:

$$x^* \equiv \log_{10} \frac{\Delta P D^2}{4 \rho_w v_w^2} \quad (8.8a)$$

$$y^* \equiv \log_{10} \frac{\tau_w D^2}{4 \rho_w v_w^2} \quad (8.8b)$$

Alternatively, x^* and y^* can be expressed in the form

$$x^* = \log_{10} \left[\frac{C_p}{8} \frac{\rho_e}{\rho_w} R_D^2 \right] , \quad (8.8c)$$

$$y^* = \log_{10} \left[\frac{C_f}{8} \frac{\rho_e}{\rho_w} R_D^2 \right] . \quad (8.8d)$$

where C_p = Preston-tube pressure coefficient
 $= (P_{pt} - P_w) / (.5 \rho_e u_e^2)$,

C_f = local skin friction coefficient $= \tau_w / (.5 \rho_e u_e^2)$,
and

R_D = Preston-tube Reynolds number

It was decided to try a straight-line¹ correlation for laminar boundary layers in analogy with Equation (8.7), since it was expected that the behaviour of a laminar sublayer is similar to that of the laminar boundary layer.

¹Later investigation showed that using a second-order function did not improve the curve-fitting accuracy.

8.3 The Curve-Fitting Program

The computer program utilized for the curve fitting is called CURFIT. After applying Equation (3.1), the Preston-tube pressure data is read in, together with other parameters like P_w , C_f , ρ_w , ν_w , and U_e obtained from the Wu and Lock [4] and the STANS [23] computer programs.

The probe characteristic length, D , was first taken to be equal to the height of the probe, i.e., 0.0097" (See Figure 2). But since Patel's correlations were based on round probes, it was decided to use an equivalent diameter of the probe. This was done by assuming the probe face to be an ellipse with major and minor axes

$$2a = 0.0138 + 0.004 = 0.0178" \text{ and}$$

$$2b = 0.0097", \text{ respectively.}$$

Then the equivalent circle has an area of

$$\frac{\pi}{4} D_{eq}^2 = \pi ab \\ \therefore D_{eq} = \sqrt{4ab}$$

$$D_{eq} = 0.01314"$$

The program then calculates x^* and y^* for each observation point*, and via a curve-fitting package prepared by Dr. Chandler [10] at Oklahoma State University, it fits the values of x^* and y^* to a straight line of the form

$$y^* = Ax^* + K \quad (8.9)$$

*Observation points were taken 0.5" apart down to the end of the laminar portion of the boundary layer.

where A (slope) and F (y-intercept) are constants to be determined by the program.

8.4 Results and Improvements

The resulting straight-line fit to all points was found to be

$$y^* = 0.632 x^* + 0.415 \quad (8.10)$$

with a root-mean-square error^a of 1.2%. This error was considered unsatisfactory.

It was assumed that the reason for this data scatter is the correlation model (8.9) does not account for variable property effects. These effects can be accounted for by introducing the reference temperature, T' , into the correlation. At this temperature, average values for density and viscosity can be calculated. Tetervin [18] suggested that to transfer the incompressible skin-friction relation of Ludwig and Tillman [19] into compressible form, two parameters need to be included, namely \bar{M}_e and T'/T_e . He and numerous other investigators have modeled the effects of these two parameters by introducing density and viscosity at a reference temperature. Although Allen [20] selected the reference temperature of Sommer and Short [13], we have chosen to use Eckert's formula for T' as defined in Equation (C.3). Also,

^a defined as

$$\left\{ \frac{\sum_{\text{all points}} \left(\frac{y^*_{\text{STAN5}} - y^*_{\text{CURFIT.}}}{y^*_{\text{STAN5}}} \right)^2}{\text{No. of points}} \right\}^{1/2}$$

the use of the incompressible Bernoulli equation to calculate u_{Pt} , Equation (8.2), is not accurate. Assuming isoenergetic flow ($T_{t,Pt} = T_{t,e}$) across the boundary layer, u_{Pt} can be calculated more accurately as follows:

$$P_{Pt}/P_w = (1 + \frac{\gamma-1}{2} M_{Pt}^2)^{\gamma/(\gamma-1)}$$

$$\text{or } M_{Pt}^2 = \frac{2}{\gamma-1} \left[(P_{Pt}/P_w)^{(\gamma-1)/\gamma} - 1 \right] \quad (8.11)$$

$$\text{and } u_{Pt}/U_e = \frac{M_{Pt}}{M_e} \sqrt{\frac{T_{Pt}}{T_e}} = \frac{M_{Pt}}{M_e} \sqrt{\frac{T_{Pt}}{T_{t,Pt}}} \sqrt{\frac{T_{t,e}}{T_e}} \sqrt{\frac{T_{t,Pt}}{T_{t,e}}}$$

$$\therefore u_{Pt}/U_e = \frac{M_{Pt}}{M_e} \left(\frac{1 + \frac{\gamma-1}{2} M_e^2}{1 + \frac{\gamma-1}{2} M_{Pt}^2} \right)^{1/2} \quad (8.12)$$

and x^* is now defined as

$$x^* = \log_{10} (u_{Pt} D^2 / 4 P_w^2) \quad (8.13)$$

Thus, the improved model is in the form

$$y^* = A x^* + B \log(T'/T_e) + K$$

The resulting correlation is

$$y^* = 0.655 x^* + 2.095 \log_{10}(T'/T_e) - 0.895 \quad (8.14)$$

with an rms error of 1%. To further improve the fitting accuracy, a quadratic model of the form

$$y^* = A x^{*2} + B x^* + C \log_{10}(T'/T_e) + K$$

was tried. The result is

$$y^* = 0.273 x^{*2} - 2.618 x^* + 1.645 \log_{10}(T'/T_e) + 8.921 \quad (8.15)$$

with an rms error of 0.85%. Equation (8.15) can be written in the form

$$C_f = 6.67 \times 10^9 \frac{P_w}{P_e} 10^{\log_{10}^2 (u_{Pt} D / 2 P_w) 0.546} \left(\frac{U_{Pt} D}{2 P_w} \right)^{-5.236} \left(\frac{T'}{T_e} \right)^{1.645} R_D^{-2} \quad (8.16)$$

which has an rms error of 0.85%. Figure 7 shows the data scatter in of C_f . Figure 8 compares the recommended correla-

tion (8.15) with the data. The term z^* is defined as

$$z^* = 0.273 x^{*2} - 2.618 x^* + 1.645 \log_{10}(T'/T_e)$$

The extraneous data, which appears above the 10³ line in Figure 7, corresponds to a Mach number of 0.80 and Re_{ft} of three and four million. It is speculated that these data are a result of the formation of a transonic shock on the stem of the flow-angularity probe (e.g. see Reference 8) which affects the measured values of P_{ref} and thus P_{pt} . Discarding only this particular data, a new fit results in the following equation.

$$y^* = 0.0942 x^{*2} - 0.438 x^* + 2.023 \log_{10}(T'/T_e) + 2.272 \quad (8.17)$$

The corresponding rms error in C_f is 4.93%. Thus, Equation (8.17) is the recommended correlation for relating C_f and P_{pt} within subsonic, compressible laminar boundary layers.

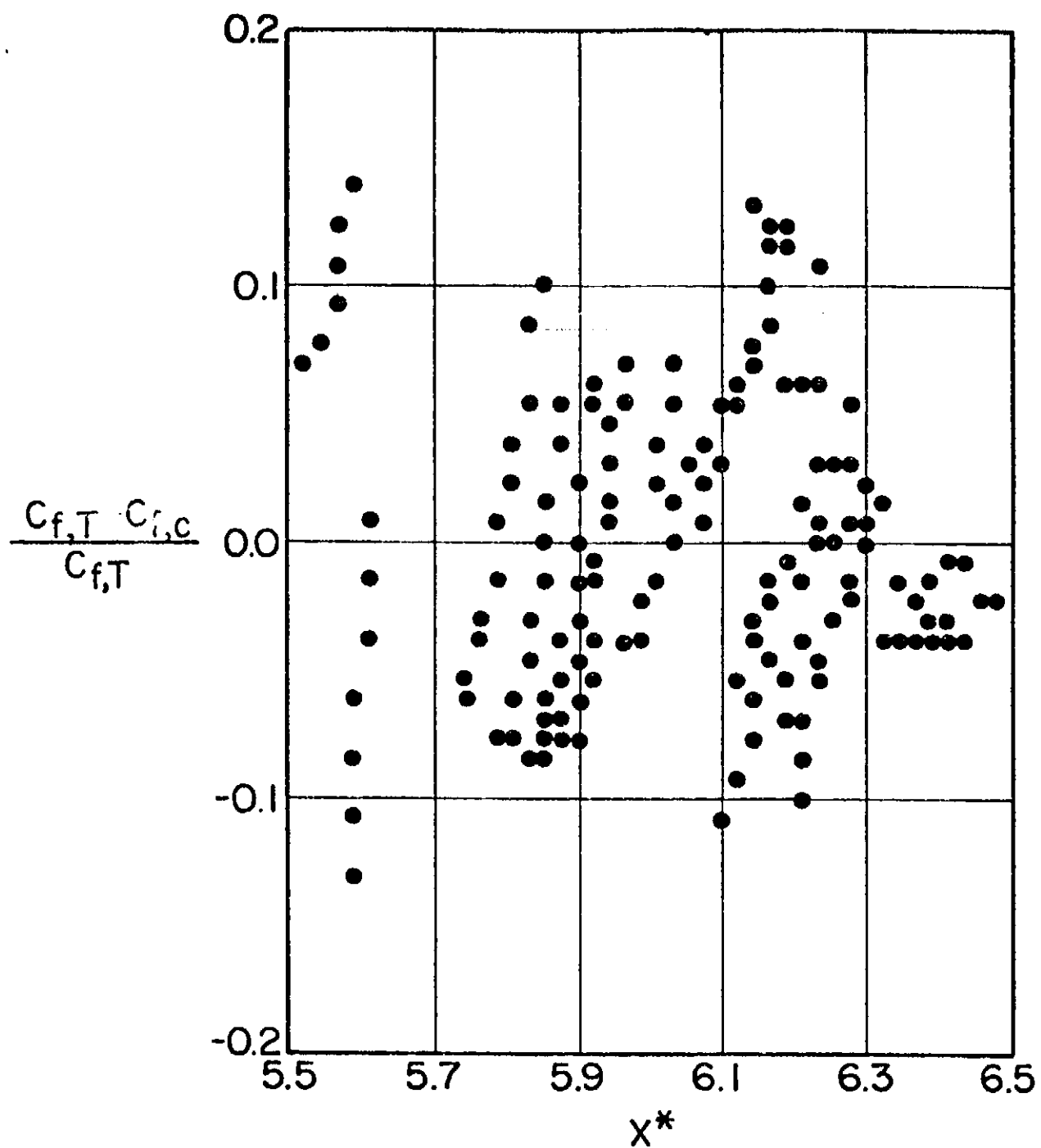


Figure 7. Deviation of Predicted Skin-Friction Coefficient by Eqn. (8.15) from Theoretical Values

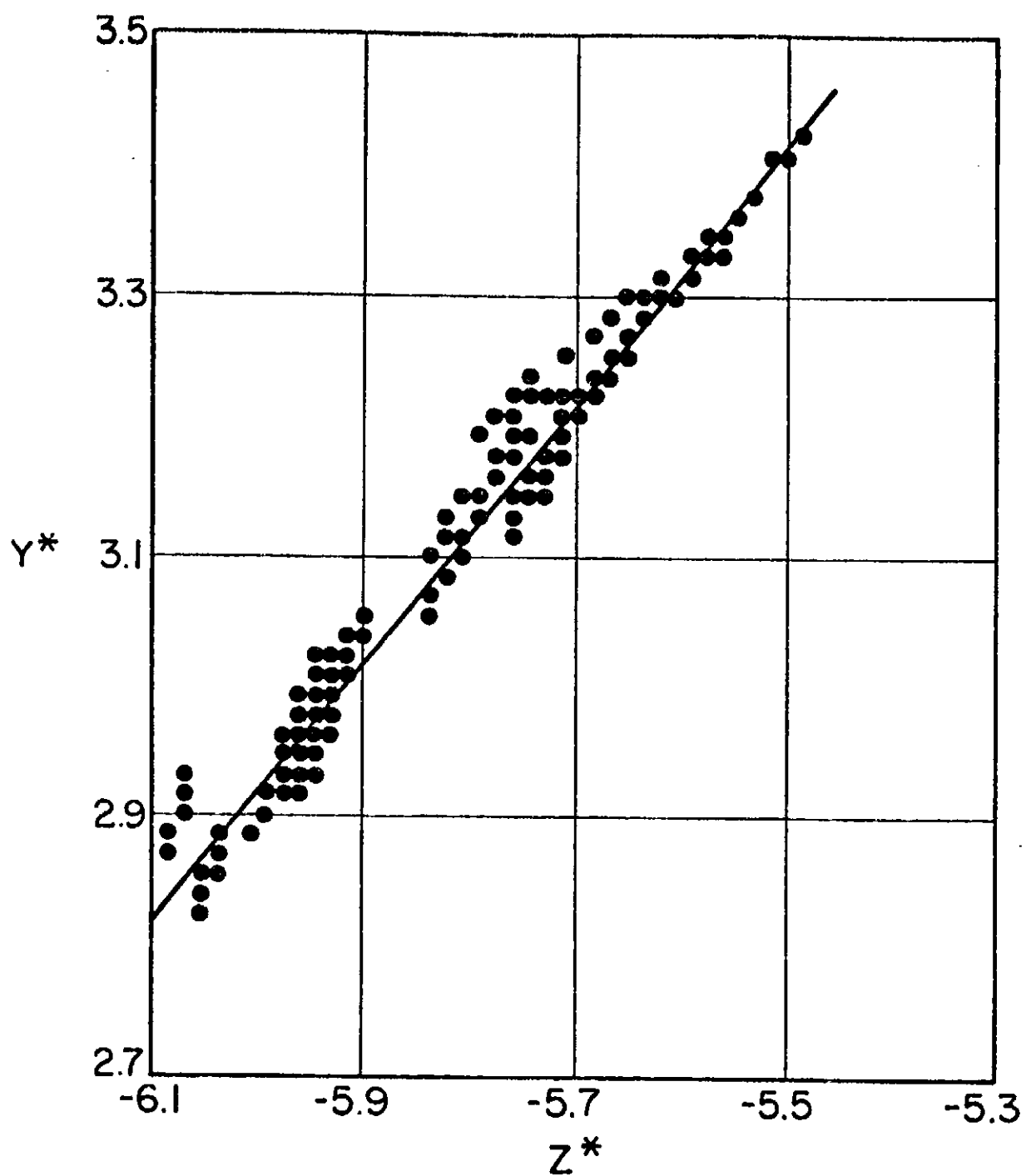


Figure 8. Data Collapse About Correlation (8.15)

8.5 General Remarks

a. The increase of D discussed in section 8.3, resulted in a better fit. This can be explained as follows : In the process of deriving Equation (8.4), the non-dimensional effective center of the probe, $k_{\text{eff}} \times$ is assumed to be unity. Patel [16] and Prozorov [22] and others, e.g. Chue [17], have found that $0.55 \leq y_{\text{eff}}/D \leq 0.65$. Thus, writing Equation (8.4) in the form

$$\frac{\Delta P}{r_w} g \left[\frac{u^* D_{\text{eq}}}{2 v} \right], D_{\text{eq}} \approx 1.3D$$

is equivalent to assuming that the average value of $y_{\text{eff}} = 1.3 D/2 = 0.65 D$, or equivalently $k_{\text{eff}} = 1.3$.

The better fit is an indication of the strong effect of the probe geometry expressed by R_D . One can also conclude that k_{eff} is a function of R_D . This conclusion was postulated before by Preston [21]. Patel [16] and Prozorov [22] showed that k_{eff} is a function of $u_{\text{pt}} D/\nu$.

b. Although the assumption that k_{eff} is a constant works well, k_{eff} is not a constant in fact. This can be seen in Figure 6. It increases slowly with x . It can be shown that a constant k_{eff} requires that the coefficient of x^* in the correlation be 0.5. The higher coefficient in Equation (8.10) confirms that k_{eff} is not a constant. Assuming a Blasius type profile, it is shown in Appendix D that $k_{\text{eff}} \propto (x/D)^{.337}/(Re_x)^{.355}$.

c. The correlation (8.15) is true for body geometries other than the cone since it is based on local variables. It

accounts for heat transfer conditions since it includes the temperature ratio T^*/T_e . It is also thought to be valid for pressure gradients since it is based on conditions near the wall. Thus, it is considered to be a general equation for estimation of skin-friction coefficients in subsonic, laminar boundary layers.

d. In an attempt to improve the curve-fit, we tried various calibration models. Among them were the following results :

$$y^* = 0.102 x^* - 0.232 \log_{10} M_\infty + 0.815 \log_{10} Re_{ft} \\ - 0.867 \log_{10} \frac{D}{L} - 3.458 \quad (8.18a)$$

with an rms error of 0.27%,

$$y^* = 0.011 x^* - 0.582 \log_{10} (1+M_\infty^2) + 0.481 \log_{10} Re_x \\ - 1.972 \log_{10} \frac{D}{L} - 1.554 \quad (8.18b)$$

with an rms error of 0.06%, and

$$\log_{10} \frac{1}{c_f} = 0.002 \log_{10} [(P_{pt} - P_\infty/q_\infty)] + 0.024 \log_{10} (1+M_\infty^2) \\ + 0.501 \log_{10} (Re_{ft} D \frac{x}{L}) + 1.688 \quad (8.18c)$$

with an rms error of 0.02%. Though the accuracy of the fit became better and better, the dependence on x^* and the Preston-tube measurements became less and less. This means that STAN calculations were correlated in these calibration models rather than the experimental data.

The use of freestream parameters (M_∞, Re_{ft}) in correlations (8.18a,b,c) limits their use to the 10-degree cone measurements, i.e., the coefficients of M_∞ and Re_{ft} in these correlations are not universal. To correct for that, the local Mach number M_e and Re_x should be used.

e. The calibration models used by Bradshaw and Unsworth, Allen, Fenter and Stallmach, and Patel which were reported by Allen in his survey report [20] were all tried for the present laminar data. It was found that none of them was competitive with our correlation in terms of the rms error in skin-friction coefficient. Allen's 2nd-degree model fitted the laminar data with an rms error in C_f of 8.6%.

f. Bradshaw and Unsworth [23] have criticized Allen's use of the reference temperature to evaluate density and viscosity in the classical law-of-the-wall. Rather than replace the conventional evaluation of properties at the wall, we have followed the procedure by Teterivin [18] and others to obtain a compressible equation for C_f by simply multiplying an incompressible equation for C_f by the ratio of T^*/T_e raised to some exponent. Here we have determined the exponent via a curve fit of the data. Thus, we are partially accounting for Bradshaw and Unsworth's objection. However, their second objection still applies to our analysis in that the reference temperature method is based on zero-pressure-gradient flows and has an unknown range of validity for flows with pressure gradients.

8.6 Prozorov Correlation

Assuming a relatively small height of the Preston-tube, Prozorov [22] expanded the velocity u about the wall using MacLaurin's series and reached the following simple correlation for incompressible laminar boundary layers.

$$C_f = \frac{1}{q_e} \left(\frac{\mu u_{pt}}{y_{eff}} - \frac{1}{2} y_{eff} \frac{dp}{dx} \right) \quad (8.19)$$

He analytically verified Equation (8.19) for round and rectangle openings of the probe (for which y_{eff} can be theoretically calculated).

Correlation (8.19) has the advantage that it can be used for high pressure gradients*, and the disadvantage that y_{eff} must be known a priori.

It is also limited to incompressible flows.

It is worth mentioning that Prozorov's paper is the only study found in the literature that discusses correlating Preston-tube data with theoretical laminar shear stress.

*All the cases investigated in this study had small favorable dp/dx .

CHAPTER IX

CONCLUSIONS

1. The Wu and Lock computer program is an accurate and reliable way of calculating the inviscid flow field about a sharp cone at transonic speeds.

With the added subroutines, the program is now capable of calculating the inviscid pressure and velocity distribution along a conical ray, corresponding to the Preston tube survey, for arbitrary combinations of pitch and yaw angles. It also calculates compressible initial profiles based on similarity theory and the supersonic laminar cone rule; this information is used to start the boundary layer computations.

2. The STANS computer code does not work satisfactorily when the flow angles are significant. It was found that its calculations were insensitive to changes in the flow angles when other parameters were kept the same. This limits its utility.

3. It is possible to correlate skin friction and experimental Preston-tube pressure measurements in the simple form (8.17).

4. The non-dimensional effective center of the Preston tube, k_{eff}/x , is not a constant value but rather increases with x and decreases with k_x .

CHAPTER X

SUPPLEMENTARY OBSERVATIONS

1. A 3-dimensional boundary-layer computer code is needed to continue investigation of the role of pitch and yaw angles on the correlation of Preston-tube data and skin friction.
2. The laminar correlation needs to be verified in supersonic flows and also for free-flight conditions for which the wall temperature seldom equals the adiabatic wall temperature.
3. By using the measured Preston-tube pressures at the end of transition, the correlation of Allen [20] can be used to initiate computation of the fully-developed turbulent boundary layers on the cone. This avoids tackling the development of a skin-friction correlation for the boundary-layer transition region until the laminar and turbulent correlations are established.
4. The laminar correlation may be connected with Allen's and/or Bradshaw and Unsworth's [20] correlations for turbulent boundary layers in order to model boundary-layer transition.
5. In order to verify and make use of Prozorov's [22] findings, a method is required that relates the Preston-tube pressure to the geometry of the probe. One way of doing this

is by curve-fitting the computed values of k_{eff} (obtained from plots similar to Figure 6) with x and Re_x .

BIBLIOGRAPHY

- (1) NASA/Ames 11-Ft Transonic Wind Tunnel Measurements. NASA/Ames Research Center, Moffet Field, California. March 1975.
- (2) Crawford, M. E. and W. M. Kays, "STANS - A Program For Numerical Computation of Two-Dimensional Internal/External Boundary Layer Flows". Report No. HMT-23, Department of Mechanical Engineering, Stanford University. December 1975.
- (3) Patankar, S. V. and D. B. Spalding, Heat and Mass Transfer in Boundary Layers. 2nd Edition. Intertext Books, London. 1970.
- (4) Wu, J. and R. C. Lock, "A Theory for Subsonic and Transonic Flow Over a Cone - With and Without Small Yaw Angle". Technical Report RD-74-2, U. S. Army Missile Command. December 1973.
- (5) Huprikar, A. G., "Evaluation Method for Transonic Cone Boundary Layer Transition Data by Means of Computer Simulation". Oklahoma State University. December 1978.
- (6) Davis, J. W., "Optimization of Wave Cancellation in Variable Porosity Transonic Wind Tunnel Flows". George C. Marshall Space Flight Center, Alaska. November 1973.
- (7) Goin, K. L., "The History, Evolution and Use of Wind Tunnels". AIAA Student Journal. February 1971.
- (8) Reed, T. D., T. C. Pope and J. M. Cooksey, "Calibration of Transonic and Supersonic Wind Tunnels". NASA CR 2920. November 1977.
- (9) Dougherty, N. S., Jr., Private Communication. November 1979.
- (10) Chandler, J. P. and L. W. Jackson, "Subroutine MARQ, Version 2.6, A.N.S.I. Standard FORTRAN". WATFIV Library, University Computer Center, Oklahoma State University. February 1979.

- (11) Dunn, M., R. Jones and M. Zissen, "Computer Program for Calculation of Effective Angle of Attack and Location of Windward Element". Report TIAD 661. Interdepartmental Communication. Lockheed Aircraft Corporation. 14 November 1963.
- (12) Equations, Tables and Charts for Compressible Flow. Ames Research Staff. NACA Report 1135. Ames Aeronautical Laboratory, Moffet Field, California.
- (13) White, F. M., Viscous Fluid Flow, McGraw-Hill Book Co. New York. 1974.
- (14) Whitfield, J. D. and N. S. Dougherty, Jr., "A Survey of Transition Research at AFEDC". AGARD Conference Proceeding No. 224.
- (15) Dougherty, N. S., Jr. and D. F. Fisher, "Boundary Layer Transition on a 10-Degree Cone : Wind Tunnel/Flight Data Correlation". AIAA 18th Aerospace Sciences Meeting. Pasadena, California. January 14-16, 1980.
- (16) Patel, V. C., "Calibration of the Preston Tube and Limitations on its Use in Pressure Gradients". J. Fluid Mechanics, Vol. 23, pp. 185-208. 1965.
- (17) Chue, S. H., "Pressure Probes for Fluid Measurement". Engg. Aerospace Sci., Vol. 16, No. 2, pp. 147-221. 1975.
- (18) Teterivin, N., "A Transformation between Axisymmetric and two-Dimensional Turbulent Boundary Layers". AIAA Journal, Vol. 8, No. 5, pp. 985-987. May 1970.
- (19) Schlichting, H., Boundary Layer Theory, McGraw-Hill Book Co. 1968.
- (20) Allen, J. M., "Reevaluation of Compressible-Flow Preston Tube Calibrations". NASA TM X-3488. February 1977.
- (21) Preston, J. H., "Determining Skin Friction with Pitot Tubes". J. Royal Aeronautical Society, 54, 518. 1954.
- (22) Prozorov, A. G., "Determinations of the Skin Friction in the Boundary Layer with a Small Pitot Probe". Fluid Mechanics Soviet Research, Vol. 5, No. 6. November-December 1976.

- (23) Bradshaw, P. and K. Unsworth, "Comment on Evaluation
of Preston Tube Calibration Equations in
Supersonic Flow". AIAA Journal, Vol. 12, No. 9,
pp. 1293-1296. September 1974.

APPENDIX A

AZIMUTH ANGLE CALCULATION

In this appendix are presented the equations developed by Dunn et al [11] to locate the windward element. Figure 9 is a schematic of a typical vehicle at angle of attack which defines the parameters used in this appendix. As illustrated, the angles of pitch and yaw are measured with respect to the freestream velocity vector. It should be noted that the relationship utilized to determine the location of the windward element is sensitive to calculation accuracy. For this reason, double precision is used in the computer subprogram ANGLES. The pitch and yaw angles are restricted to magnitudes less than 90 degrees.

The first step is to evaluate the angle between the vehicle axis and the resolved yaw vector. This angle will be denoted by ϕ .

$$\sin(\phi) = c/f$$

$$\tan(\phi) = c/d$$

$$\sin(\alpha) = c/e$$

$$\tan(\alpha) = c/a$$

$$\sin(\alpha)/\sin(\phi) = (c/e)/(c/f) = t/e$$

$$\tan(\alpha)/\tan(\phi) = (c/a)/(c/d) = d/a$$

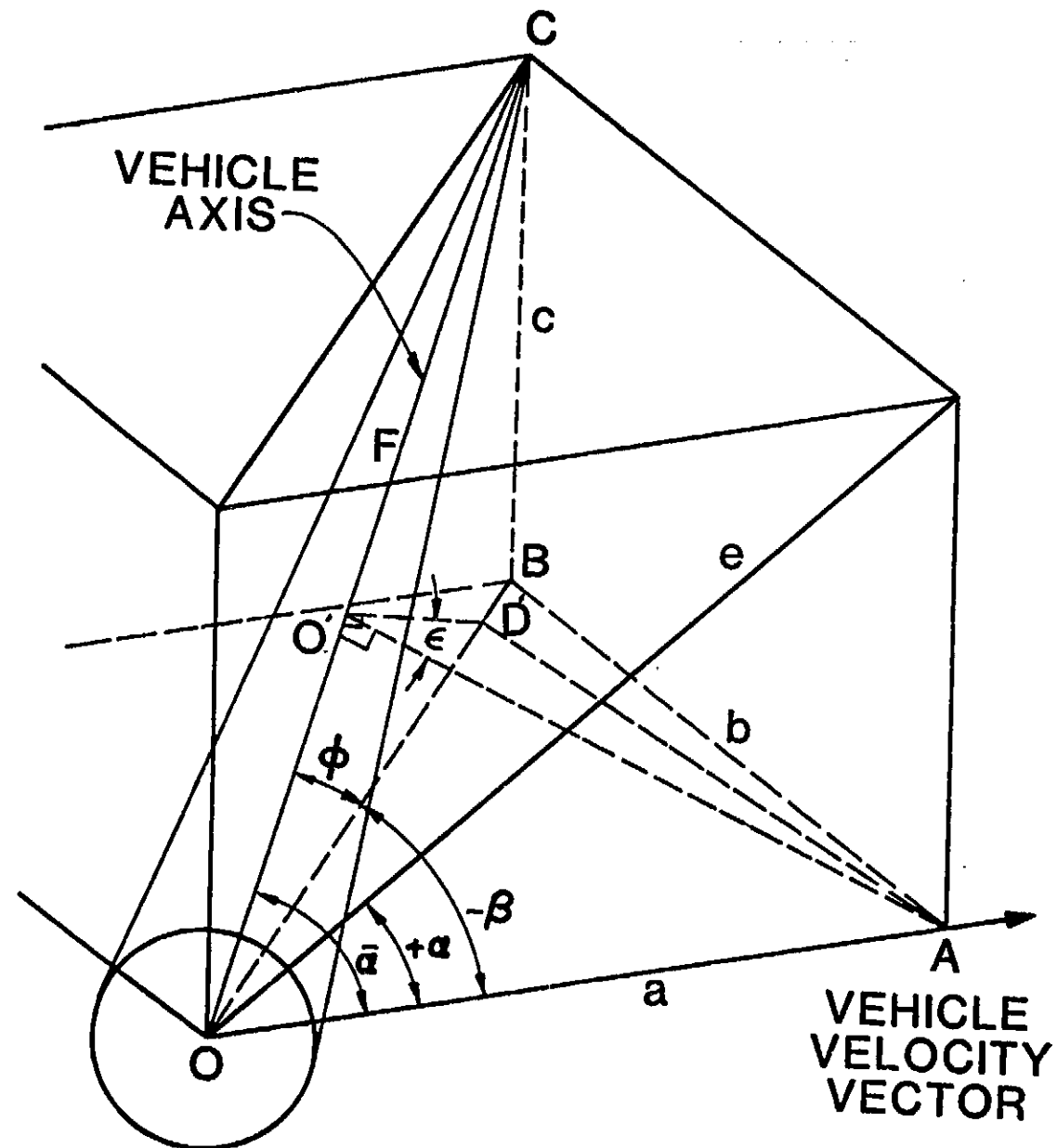


Figure 9. Schematic of Flow Angles

ORIGINAL PAGE IS
OF POOR QUALITY

$$\cos(\beta) = a/d$$

$$\text{Thus } \tan(\phi) = (a/d) \tan(\alpha) = \cos(\beta) \tan(\alpha)$$

$$\tan(\phi) = \cos(\beta) \tan(\alpha) \quad (\text{A.1})$$

Now the angle $\bar{\alpha}$ can be calculated as follows :

$$d/f = \cos(\phi), \cos(\bar{\alpha}) = a/f = (a/d)(d/f)$$

$$\therefore \cos(\bar{\alpha}) = \cos(\beta) \cos(\phi), 0 < \bar{\alpha} < 90 \quad (\text{A.2})$$

Equation (A.2) determines the angle $\bar{\alpha}$ which is denoted as the effective angle of attack.

At this point, we want to find the angle that the windward vector makes with the vehicle axis. The following results can be obtained from Figure 9.

$$\cos(\epsilon) = (O^*D^*)/(O^*A)$$

$$O^*A = a \sin(\bar{\alpha})$$

$$O^*O = a \cos(\bar{\alpha})$$

$$\tan(\phi) = (O^*D^*)/(O^*O)$$

$$\cos(\epsilon) = (O^*D^*)/a \sin(\bar{\alpha}) = (O^*O)\tan(\phi)/a \sin(\bar{\alpha})$$

$$\cos(\epsilon) = a \cos(\bar{\alpha}) \tan(\phi)/a \sin(\bar{\alpha})$$

$$\therefore \cos(\epsilon) = \cot(\bar{\alpha}) \tan(\phi) \quad (\text{A.3})$$

An alternate expression for calculating ϵ can be formed by substituting Equation (A.1) for $\tan(\phi)$

$$\cos(\epsilon) = \cot(\bar{\alpha}) \cos(\beta) \tan(\alpha)$$

APPENDIX B

CALCULATION OF FREESTREAM PROPERTIES

Values of M_∞ , q_∞ and Re_{ft} are specified for a given wind tunnel setting. From these values, all properties of the freestream can be calculated as follows :

1. Obtain the freestream total pressure $P_{t,\infty}$ as follows :

$$q_\infty = \frac{1}{2} \rho_\infty U_\infty^2 = \frac{1}{2} \rho_\infty M_\infty^2 (\gamma P_\infty / \rho_\infty) \\ = \gamma M_\infty^2 P_\infty / 2 \quad (B.1)$$

$$P_{t,\infty} = \frac{P_{t,\infty}}{P_\infty} \cdot \frac{P_\infty}{q_\infty} \cdot q_\infty \\ = 2 q_\infty \left(1 + \frac{\gamma-1}{2} M_\infty^2\right)^{\gamma/(\gamma-1)} / \gamma M_\infty^2 \quad (B.2)$$

Note that the total pressure and temperature are constant for isentropic, subsonic flow.

2. Obtain the freestream static temperature as follows :

$$\frac{M_\infty Re_{ft}}{q_\infty} = \frac{U_\infty}{\sqrt{\gamma R T_\infty}} \cdot \frac{\rho_\infty U_\infty}{\mu_\infty} \cdot \frac{2}{\rho_\infty U_\infty^2} = \frac{2}{\mu_\infty \sqrt{\gamma R T_\infty}} \\ = \frac{2 (T_\infty + 198.6)}{2.27 \times 10^{-8} T_\infty^{1.5} \sqrt{\gamma R T_\infty}} \\ \therefore \left(\frac{M_\infty Re_{ft}}{q_\infty} \cdot \frac{2.27 \times 10^{-8} \gamma R}{2} \right) T_\infty^2 - T_\infty - 198.6 = 0 \quad (B.3)$$

Where Sutherland's relation is used for μ_∞ .

3. Using Equations (B.1) and (B.3), ρ_∞ can be obtained from the perfect gas relation :

$$\rho_\infty = P_\infty / R T_\infty \quad (B.4)$$

4. Also the total temperature can be found using the isentropic relation :

$$T_t = T_\infty \left(1 + \frac{\gamma-1}{2} M_\infty^2 \right) \quad (B.5)$$

This procedure is automated in subroutine DIST of the extended Wu and Lock program described in Chapter V. The listing of the routine can be found in Appendix F.

APPENDIX C

CALCULATION OF INITIAL PROFILES

Since STANS is a forward-marching, finite-difference program, starting profiles of velocity and total enthalpy are required to calculate subsequent velocity and total enthalpy profiles along the cone. Care should be taken, therefore, in calculating these initial profiles. However, the effect of the starting profile on the calculations becomes small after a certain developmental distance, as shown in Figure 1.

The edge velocity distribution can be expressed [13] as follows

$$U_e = c x^n \quad (C.1)$$

Where c and n are constants. Fitting Equation (C.1) to typical edge velocities near the tip of the cone, as obtained from the extended Wu and Lock program¹, results in $n = 0.0047$.

The pressure gradient parameter for a conical flow, β_c , is related to the inviscid velocity distribution [13] by

$$\beta_c = \frac{2n}{3+n} = 0.003128.$$

This in turn corresponds to a wedge flow with

$$n_w = n_c/3 = 0.00157.$$

¹Case analyzed here was Case 40.547.

Examination of Figure 4-11 of White [13] indicates that the solution for $f(\eta)$ corresponding to $\beta=0$ is expected to be good. Therefore, the tabulated solution for Blasius flow may be used to specify the initial profiles. The normal distance y_c can be calculated now from

$$y_c = y_B / \sqrt{3}$$

$$\therefore y_c = n_B / \left[\frac{3 U_e}{2 v' x} \right]^{1/5} \quad (C.2)$$

Where v' is the kinematic viscosity evaluated at the reference temperature T^* as will be shown now. One can obtain Equation (C.2) using Mangler transformation.

An expression for the reference temperature across the boundary layer is given by Eckert's formula [13] :

$$T' = T(0.5 + 0.039 M_e^2 + 0.5 T_w/T) \quad (C.3)$$

Where $T = T_t / (1 + \frac{\gamma-1}{2} M^2)$ (C.4)

and $T_w = T_{aw} = T(1 + r \frac{\gamma-1}{2} M^2)$ (C.5)

Where $r = (\text{Pr})^{1/2}$ for laminar boundary layer, and
 $= (\text{Pr})^{1/3}$ for turbulent boundary layer.

The values of local Mach numbers M_e and the total temperature T_t are calculated by the extended Wu and Lock program. Prandtl number is taken to be 0.72 for air.

Now μ' can be calculated using Sutherland's relation

$$\mu' = 2.27 \times 10^{-8} \frac{(T')^{1.5}}{T' + 198.6} \quad (C.6)$$

To obtain ν' , ρ' is calculated using the perfect gas relation

$$\rho' = P_w / R T' \quad (C.7)$$

Where the static pressure P_w is calculated in the main Wu and Lock program.

Therefore, from (C.6) and (C.7), ν' can be calculated,

$$\nu' = \mu'/\rho' \quad (C.8)$$

Substitution in (C.2), yields a table of y_c vs. η_B . From the Blasius solution for $t^* = u/U_e$, we can obtain a table of u vs. η_B . Thus the initial velocity profile is specified.

The total enthalpy is defined as

$$h_t = h + \frac{u^2}{2 g_c J}$$

$$= c_p T + \frac{u^2}{2 g_c J} \quad \text{for } c_p = \text{constant (C.9)}$$

The distribution of T through the boundary layer may be approximately expressed [13] as

$$T \approx T_w + (T_{aw} - T_w) \frac{u}{U_e} - \frac{r u^2}{2 c_p g_c J}$$

Substitution into (C.9) gives

$$h_t = c_p [T_w + (T_{aw} - T_w) \frac{u}{U_e}] + \frac{(1-r) u^2}{2 g_c J}$$

With the assumption $T_w = T_{aw}$, this equation reduces to

$$h_t = c_p T_w + \frac{(1-r) u^2}{2 g_c J} \quad (C.10)$$

T_w was calculated via the Wu and Lock program, and the initial stagnation profile was defined by Equation (C.10).

APPENDIX D

FUNCTIONAL DEPENDENCE OF THE EFFECTIVE CENTER OF THE PROBE

For simplicity, we will derive an expression for k_{eff} for incompressible flow over a flat plate. The correlation (8.14) reduces in this case to

$$C_f \sim C_p^{0.655} R_D^{0.69} \quad (\text{D.1})$$

where $C_f = \tau_w / (0.5 \rho u^2)$,

$$C_p = \Delta P / (0.5 \rho u^2),$$

$$R_D = U D / v = (U x / v) D / x = Re_x D / x. \quad \text{Since } \Delta P = \frac{1}{2} \rho u_{pt}^2$$

C_p can be written in the form

$$C_p = (u_{pt}/U)^2 = (f')^2 \text{ at } \eta_{\text{eff}},$$

where $f' = 1^{\text{st}} \text{ derivative of the Blasius function w.r.t. } \eta$,
and

$$\eta_{\text{eff}} = y_{\text{eff}} \sqrt{U/2v} x \sim k_{\text{eff}} D \sqrt{Re_x} / x.$$

Since the height of the probe is very small (0.0097"), all the laminar boundary-layer data was obtained within the lower 40% of the layer thickness. In this region $f' \sim \eta$ is valid.

Therefore, C_p can be expressed as

$$C_p \sim \eta_{\text{eff}}^2 \sim k_{\text{eff}}^2 D^2 Re_x / x^2. \quad (\text{D.2})$$

Substituting relation (D.2) into (D.1) gives

$$C_f \sim k_{\text{eff}}^{1.31} Re_x^{-0.035} \left(\frac{x}{D}\right)^{-0.441} \quad (\text{D.3})$$

The well-known relation for C_f in this case is

$$C_f \sim Re_x^{-0.5} \quad (D.4)$$

Comparing (D.3) and (D.4), the following equation is obtained for k_{eff} .

$$k_{eff} \sim Re_x^{-0.355} \left(\frac{x}{D}\right)^{0.337} \quad (D.5a)$$

$$\text{Or alternatively, } k_{eff} \sim Re_x^{-0.018} R_D^{-0.337} \quad (D.5b)$$

Again, relations (D.5a,b) are only valid for incompressible flow over a flat plate and are presented here only to demonstrate that y_{eff} is not a constant.

APPENDIX E
RAW DATA USED FOR SKIN-FRICTION
CORRELATION

ORIGINAL PAGE IS
OF POOR QUALITY

POINT NO.	X INF	Y INF	Z INF	X	DELTA P	PINF	UE	RHCH	RHCE	NW	NUE	THEIA	CF
1	3.63	3.52E	3.7	585.3	4.5	323.6	2325.0	636.3	3.084127	0.086915	0.14414E-03	0.13046E-03	0.0001065
2	3.63	2.51E	3.7	585.3	5.3	326.5	2325.0	636.3	0.084103	0.089896	0.14419E-03	0.13047E-03	0.0001123
3	3.63	2.51E	3.7	586.0	5.5	263.7	2225.0	636.9	0.084154	0.086883	0.14422E-03	0.13045E-03	0.0001174
4	3.63	2.52E	3.7	586.0	6.3	279.4	2325.0	637.2	0.094558	0.088869	0.14427E-03	0.13050E-03	0.0001228
5	3.63	2.52E	3.7	586.0	6.5	268.0	2325.0	637.5	0.084554	0.088855	0.14426E-03	0.13051E-03	0.0001278
6	3.63	2.52E	3.7	586.0	7.3	255.2	2225.0	637.8	0.064334	0.088814	0.14429E-03	0.13052E-03	0.0001324
7	3.63	2.52E	3.7	586.0	7.5	246.6	2225.0	638.1	0.084521	0.088829	0.14431E-03	0.13054E-03	0.0001370
8	3.63	2.52E	3.7	586.0	7.7	246.3	2225.0	638.1	0.084518	0.088826	0.14432E-03	0.13055E-03	0.00014123
9	3.63	2.52E	3.7	586.0	7.9	279.3	2325.0	640.0	0.067564	0.071410	0.18143E-03	0.16422E-03	0.0001191
10	3.63	2.52E	3.7	586.0	8.1	252.3	1893.0	640.9	0.067546	0.071397	0.18148E-03	0.16424E-03	0.0001253
11	3.63	2.52E	3.7	586.0	8.3	238.1	1892.0	641.3	0.067531	0.071384	0.18152E-03	0.16426E-03	0.0001314
12	3.63	2.52E	3.7	586.0	8.5	228.1	1893.0	641.6	0.067510	0.071373	0.18159E-03	0.16428E-03	0.0001370
13	3.63	2.52E	3.7	586.0	8.7	477.3	637.0	642.0	0.067508	0.071361	0.18157E-03	0.16430E-03	0.0001427
14	3.63	2.52E	3.7	586.0	8.9	477.0	637.0	642.1	0.067505	0.071350	0.18159E-03	0.16431E-03	0.0001483
15	3.63	2.52E	3.7	586.0	9.1	477.0	637.0	642.4	0.067483	0.071340	0.18163E-03	0.16432E-03	0.0001533
16	3.63	2.52E	3.7	586.0	9.3	477.0	637.0	642.7	0.067468	0.071330	0.18167E-03	0.16435E-03	0.0001584
17	3.63	2.52E	3.7	586.0	9.5	357.0	637.0	641.5	0.050595	0.053491	0.24196E-03	0.16428E-03	0.0001652
18	3.63	2.52E	3.7	586.0	9.7	357.0	637.0	641.8	0.050584	0.053483	0.24232E-03	0.16430E-03	0.0001713
19	3.63	2.52E	3.7	586.0	9.9	357.0	637.0	642.1	0.050573	0.053475	0.24237E-03	0.16431E-03	0.0001773
20	3.63	2.52E	3.7	586.0	10.1	357.0	637.0	642.3	0.050566	0.053469	0.24210E-03	0.16435E-03	0.0001825
21	3.63	2.52E	3.7	586.0	10.3	357.0	637.0	642.6	0.050555	0.053461	0.24212E-03	0.16438E-03	0.0001885
22	3.63	2.52E	3.7	586.0	10.5	357.0	637.0	642.8	0.050552	0.053454	0.24219E-03	0.16436E-03	0.0001936
23	3.63	2.52E	3.7	586.0	10.7	357.0	637.0	643.1	0.050542	0.053447	0.24219E-03	0.16437E-03	0.0001985
24	3.63	2.52E	3.7	586.0	10.9	357.0	637.0	643.3	0.050536	0.053440	0.24219E-03	0.21904E-03	0.0002041
25	3.63	2.52E	3.7	586.0	11.1	357.0	637.0	643.5	0.050526	0.053433	0.24216E-03	0.21906E-03	0.0002089
26	3.63	2.52E	3.7	586.0	11.3	357.0	637.0	643.7	0.050516	0.053427	0.24223E-03	0.21907E-03	0.0002137
27	3.63	2.52E	3.7	586.0	11.5	124.0	1417.0	644.2	0.053454	0.053454	0.24214E-03	0.21903E-03	0.0002174
28	3.63	2.52E	3.7	586.0	11.7	121.2	1417.0	644.3	0.053452	0.053447	0.24219E-03	0.21902E-03	0.0002217
29	3.63	2.52E	3.7	586.0	11.9	118.3	1417.0	644.3	0.053450	0.053440	0.24219E-03	0.21904E-03	0.0002258
30	3.63	2.52E	3.7	586.0	12.1	115.5	1417.0	644.3	0.053448	0.053433	0.24216E-03	0.21906E-03	0.0002295
31	3.63	2.52E	3.7	586.0	12.3	112.6	1417.0	644.8	0.053446	0.053427	0.24223E-03	0.21907E-03	0.0002332
32	3.63	2.52E	3.7	586.0	12.5	104.0	1417.0	645.0	0.053444	0.053417	0.24219E-03	0.21908E-03	0.0002369
33	3.63	2.52E	3.7	586.0	12.7	45.0	1417.0	645.2	0.053442	0.053407	0.24219E-03	0.21909E-03	0.0002406
34	3.63	2.52E	3.7	586.0	12.9	44.0	1417.0	645.3	0.053440	0.053397	0.24219E-03	0.21910E-03	0.0002443
35	3.63	2.52E	3.7	586.0	13.1	43.0	1417.0	645.4	0.053438	0.053387	0.24220E-03	0.21911E-03	0.0002480
36	3.63	2.52E	3.7	586.0	13.3	42.0	1417.0	645.5	0.053436	0.053377	0.24221E-03	0.21912E-03	0.0002517
37	3.63	2.52E	3.7	586.0	13.5	41.0	1417.0	645.6	0.053434	0.053367	0.24222E-03	0.21913E-03	0.0002554
38	3.63	2.52E	3.7	586.0	13.7	40.0	1417.0	645.7	0.053432	0.053357	0.24223E-03	0.21914E-03	0.0002591
39	3.63	2.52E	3.7	586.0	13.9	39.0	1417.0	645.8	0.053430	0.053347	0.24224E-03	0.21915E-03	0.0002628
40	3.63	2.52E	3.7	586.0	14.1	38.0	1417.0	645.9	0.053428	0.053337	0.24225E-03	0.21916E-03	0.0002665
41	3.63	2.52E	3.7	586.0	14.3	37.0	1417.0	646.0	0.053426	0.053327	0.24226E-03	0.21917E-03	0.0002702
42	3.63	2.52E	3.7	586.0	14.5	36.0	1417.0	646.1	0.053424	0.053317	0.24227E-03	0.21918E-03	0.0002739

PRINT NO.	MINF	REFIT	CINF	X	DELTAP	PINF	UE	RHOM	RHOE	VUM	NUE	THETA	CF
43	2.53	2.30E 37	302.0	7.5	116.-5	1726.0	0.526.-4	0.0611745	0.18385E-03	0.19722E-03	0.0301773	0.0308866	
44	2.53	2.31E 37	302.0	8.-3	115.5	1726.-3	0.538.-7	0.0611767	0.064219	0.19721E-03	0.0001833	0.030838	
45	2.53	2.31E 37	302.0	8.-5	112.-6	1726.-0	0.538.-9	0.0611763	0.064214	0.19722E-03	0.0001833	0.030838	
46	2.53	2.31E 37	302.0	9.-3	111.-2	1726.-0	0.535.-1	0.0611753	0.064207	0.19725E-03	0.0001833	0.030838	
47	2.53	2.31E 37	302.0	9.5	108.3	1726.-0	0.539.-3	0.0611748	0.064221	0.19726E-03	0.0001833	0.030838	
48	2.53	2.31E 37	302.0	12.-3	105.5	1726.-0	0.525.-5	0.0611744	0.064196	0.1839CE-03	0.0001956	0.030768	
49	2.53	2.31E 37	302.0	12.5	102.-6	1726.-0	0.535.-7	0.0611735	0.064193	0.19727E-03	0.0002046	0.030748	
50	2.53	2.31E 37	302.0	11.-0	101.-2	1726.-0	0.539.-9	0.0611735	0.064185	0.19728E-03	0.0002096	0.030732	
51	2.53	2.31E 37	302.0	11.-4	107.-6	1726.-0	0.542.-1	0.0611726	0.064179	0.18394E-03	0.0002144	0.030714	
52	2.75	2.41E 37	549.0	4.-5	366.-5	1598.0	0.742.-4	0.056807	0.061196	0.21734E-03	0.0002191	0.030703	
53	2.75	2.41E 37	548.0	5.-3	285.-1	1598.-0	0.742.-8	0.056785	0.061181	0.21743E-03	0.0002190	0.030964	
54	2.75	2.41E 37	548.0	5.-5	266.-6	1556.-0	0.742.-1	0.056167	0.061168	0.21753E-03	0.0001252	0.030914	
55	2.75	2.41E 37	548.0	6.-0	256.-6	1598.0	0.743.-5	0.056744	0.061153	0.21762E-03	0.0001309	0.030874	
56	2.75	2.41E 37	548.0	6.-5	246.-6	1598.0	0.743.-9	0.056738	0.061147	0.21759E-03	0.0001371	0.030834	
57	2.75	2.41E 37	548.0	7.-0	238.-1	1598.-0	0.744.-2	0.056723	0.061128	0.21765E-03	0.0001428	0.030800	
58	2.75	2.41E 37	548.0	7.-5	230.-9	1598.-0	0.744.-5	0.056712	0.061117	0.21758E-03	0.0001479	0.030772	
59	2.75	2.41E 37	548.0	8.-0	223.-6	1558.-0	0.744.-8	0.056692	0.061105	0.21777E-03	0.0001529	0.030746	
60	2.75	2.41E 37	548.0	8.-5	365.-5	1593.-0	0.740.-2	0.076907	0.076384	0.17328E-03	0.0001580	0.030722	
61	2.75	2.51E 37	687.0	5.-2	343.-6	1583.0	0.740.-6	0.070882	0.076366	0.15157E-03	0.0001661	0.030862	
62	2.75	2.51E 37	682.0	5.-5	329.-3	1483.-0	0.741.-0	0.070654	0.076346	0.17336E-03	0.0001119	0.030816	
63	2.75	2.51E 37	680.0	6.-0	313.-6	1983.-0	0.741.-3	0.076332	0.076332	0.15162E-03	0.0001173	0.030780	
64	2.75	2.51E 37	682.0	6.-5	296.-5	1593.-0	0.741.-7	0.070618	0.076316	0.17350E-03	0.0001224	0.030746	
65	2.75	2.51E 37	687.0	5.-5	161.-1	1190.-0	0.741.-1	0.042554	0.045805	0.28912E-03	0.0001518	0.030862	
66	2.75	2.51E 37	698.0	6.-0	155.-4	1190.-0	0.741.-5	0.042489	0.045795	0.28924E-03	0.0001582	0.030966	
67	2.75	2.51E 37	708.0	6.-5	151.-1	1190.-0	0.741.-8	0.042480	0.045785	0.28928E-03	0.0001650	0.030924	
68	2.75	2.51E 37	708.0	7.-0	146.-8	1190.-0	0.742.-1	0.042470	0.045776	0.28933E-03	0.0001710	0.030692	
69	2.75	2.51E 37	708.0	7.-5	142.-6	1190.-0	0.742.-4	0.042457	0.045767	0.28943E-03	0.0001768	0.030716	
70	2.75	2.51E 37	708.0	8.-0	128.-2	1190.-0	0.742.-7	0.042446	0.045759	0.28951E-03	0.0001823	0.030836	
71	2.75	2.51E 37	708.0	8.-5	135.-4	1190.-0	0.743.-0	0.042437	0.045751	0.28957E-03	0.0001879	0.030610	
72	2.75	2.51E 37	708.0	9.-0	132.-6	1190.-0	0.743.-3	0.042429	0.045742	0.28959E-03	0.0001935	0.030786	
73	2.75	2.51E 37	708.0	9.-5	128.-3	1190.-0	0.742.-6	0.042423	0.045735	0.28962E-03	0.0001988	0.030766	
74	2.75	2.51E 37	708.0	10.-0	125.-5	1190.-0	0.743.-8	0.042411	0.045728	0.28971E-03	0.0002036	0.030748	
75	2.75	2.52E 37	699.0	10.-5	122.-4	1190.-0	0.744.-1	0.042442	0.045720	0.28977E-03	0.0002086	0.030733	
76	2.49	2.4CE 37	493.9	6.-5	162.-5	3598.0	0.470.-4	0.109310	0.12605E-03	0.12611E-03	0.0001430	0.3008C6	
77	2.49	2.4CE 37	493.9	7.-0	156.-8	3598.0	0.473.-6	0.109300	0.126020	0.12067E-03	0.0001486	0.000776	
78	2.49	2.4CE 37	493.9	7.5	152.-5	3598.0	0.470.-8	0.109250	0.112C10	0.12602E-03	0.12067E-03	0.0001535	
79	2.49	2.4CE 37	493.9	8.-0	149.-7	3598.0	0.471.-0	0.109280	0.112C10	0.12603E-03	0.12068E-03	0.0001586	

POINT NO.	N.Y.F	REFI	CINF	X	DELTAP	PINF	UE	RHOE	RHOX	NUM	NUE	THETA	CF
86	2.45	2.42E-37	403.5	6.5	145.4	3558.6	6	471.2	0.112000	0.12632E-03	0.0001634	0.000704	
81	2.43	2.32E-37	246.0	6.5	162.6	2196.0	6	433.6	0.078472	0.08C454	0.15514E-03	0.0001657	
82	2.43	2.31E-37	246.0	7.0	101.2	2196.0	6	433.8	0.078467	0.080449	0.15515E-03	0.0001716	
83	2.43	2.32E-37	246.0	7.5	56.4	2196.0	6	434.0	0.078463	0.08C444	0.15515E-03	0.0001775	
84	2.43	2.32E-37	246.0	8.0	96.2	2196.0	6	434.2	0.078455	0.080438	0.15517E-03	0.0001834	
85	2.43	2.32E-37	246.0	8.5	55.5	2196.0	6	434.3	0.078460	0.080434	0.15514E-03	0.0001886	
86	2.43	2.32E-37	246.0	9.0	54.1	2196.0	6	434.5	0.078451	0.08C429	0.15517E-03	0.0001945	
87	2.43	2.32E-37	246.0	9.5	92.7	2196.0	6	434.7	0.078444	0.080424	0.15518E-03	0.0001996	
88	2.43	2.31E-37	246.0	10.0	85.5	2196.0	6	434.9	0.078437	0.08C415	0.15519E-03	0.0002048	
89	2.43	2.32E-37	246.0	10.5	86.4	2196.0	5	425.0	0.078434	0.08C415	0.15519E-03	0.0002099	
90	2.43	2.31E-37	246.0	11.0	85.5	2196.0	5	425.2	0.078438	0.080341	0.15517E-03	0.0002143	
91	2.39	2.42E-37	230.0	6.5	55.5	3651.0	6	316.8	0.13E15C	0.14C68C	0.83372E-04	0.0001434	
92	2.13	2.42E-37	230.0	7.0	89.8	3651.0	6	317.3	0.138740	0.142680	0.83379E-04	0.0001489	
93	2.32	2.42E-37	230.0	7.5	85.5	3651.0	6	317.1	0.138740	0.142673	0.83380E-04	0.0001535	
94	2.32	2.42E-37	230.0	8.0	82.7	3651.0	6	317.2	0.138740	0.142673	0.83380E-04	0.0001589	
95	2.32	2.42E-37	230.0	8.5	78.4	3651.0	6	317.4	0.138740	0.142667	0.83387E-04	0.0001638	
96	2.32	2.42E-37	230.0	9.0	396.0	2256.0	4	564.6	0.077434	0.076236	0.24032E-03	0.0001426	
97	2.32	2.42E-37	230.0	9.5	396.0	2256.0	4	564.9	0.077428	0.076232	0.24034E-03	0.0001508	
98	2.32	2.42E-37	230.0	10.0	396.0	2256.0	4	565.2	0.077420	0.076226	0.24036E-03	0.0001587	
99	2.32	2.42E-37	230.0	10.5	396.0	2256.0	4	565.5	0.077417	0.076222	0.24042E-03	0.0001662	
100	2.32	2.42E-37	230.0	11.0	396.0	2256.0	4	565.7	0.077401	0.076215	0.24043E-03	0.0001738	
101	2.32	2.42E-37	230.0	11.5	396.0	2256.0	4	566.0	0.077400	0.076210	0.24042E-03	0.0001808	
102	2.32	2.42E-37	230.0	12.0	396.0	2256.0	4	566.2	0.077458	0.076205	0.24042E-03	0.0001878	
103	2.32	2.42E-37	230.0	12.5	396.0	2256.0	4	566.5	0.077437	0.076197	0.24042E-03	0.0001945	
104	2.32	2.42E-37	230.0	13.0	396.0	2256.0	4	566.8	0.077426	0.076192	0.24042E-03	0.0002016	
105	2.32	2.42E-37	230.0	13.5	396.0	2256.0	4	567.1	0.077415	0.076187	0.24043E-03	0.0002083	
106	2.32	2.42E-37	230.0	14.0	396.0	2256.0	4	567.4	0.077400	0.076180	0.24042E-03	0.0002153	
107	2.73	2.42E-37	296.0	7.0	161.1	3536.0	5	566.2	0.074358	0.076173	0.23062E-03	0.0001978	
108	2.73	2.42E-37	296.0	7.5	538.3	6.5	219.5	737.6	0.056558	0.0663937	0.23077E-03	0.0001587	
109	2.73	2.42E-37	296.0	8.0	538.3	6.0	219.5	737.6	0.056558	0.0663937	0.23077E-03	0.0001587	
110	2.73	2.42E-37	296.0	8.5	538.3	6.5	219.5	737.6	0.056552	0.0663915	0.21583E-03	0.0001530	
111	2.73	2.42E-37	296.0	9.0	538.3	7.0	219.5	737.6	0.056551	0.0663915	0.21582E-03	0.0001579	
112	2.73	2.42E-37	296.0	9.5	538.3	7.5	219.5	737.6	0.056551	0.0663915	0.21582E-03	0.0001579	
113	2.73	2.42E-37	296.0	10.0	538.3	8.0	219.5	737.6	0.056551	0.0663915	0.21582E-03	0.0001579	
114	2.73	2.42E-37	296.0	10.5	538.3	8.5	219.5	737.6	0.056551	0.0663915	0.21582E-03	0.0001579	
115	2.73	2.42E-37	296.0	11.0	538.3	9.0	219.5	737.6	0.056551	0.0663915	0.21582E-03	0.0001579	
116	2.73	2.42E-37	296.0	11.5	538.3	9.5	219.5	737.6	0.056551	0.0663915	0.21582E-03	0.0001579	
117	2.73	2.42E-37	296.0	12.0	538.3	10.0	219.5	737.6	0.056551	0.0663915	0.21582E-03	0.0001579	
118	2.73	2.42E-37	296.0	12.5	538.3	10.5	219.5	737.6	0.056551	0.0663915	0.21582E-03	0.0001579	
119	2.73	2.42E-37	296.0	13.0	538.3	11.0	219.5	737.6	0.056551	0.0663915	0.21582E-03	0.0001579	
120	2.73	2.42E-37	296.0	13.5	538.3	11.5	219.5	737.6	0.056551	0.0663915	0.21582E-03	0.0001579	
121	2.73	2.42E-37	296.0	14.0	538.3	12.0	219.5	737.6	0.056551	0.0663915	0.21582E-03	0.0001579	
122	2.73	2.42E-37	296.0	14.5	538.3	12.5	219.5	737.6	0.056551	0.0663915	0.21582E-03	0.0001579	
123	2.73	2.42E-37	296.0	15.0	538.3	13.0	219.5	737.6	0.056551	0.0663915	0.21582E-03	0.0001579	
124	2.73	2.42E-37	296.0	15.5	538.3	13.5	219.5	737.6	0.056551	0.0663915	0.21582E-03	0.0001579	
125	2.73	2.42E-37	296.0	16.0	538.3	14.0	219.5	737.6	0.056551	0.0663915	0.21582E-03	0.0001579	
126	2.73	2.42E-37	296.0	16.5	538.3	14.5	219.5	737.6	0.056551	0.0663915	0.21582E-03	0.0001579	
127	2.73	2.42E-37	296.0	17.0	538.3	15.0	219.5	737.6	0.056551	0.0663915	0.21582E-03	0.0001579	
128	2.73	2.42E-37	296.0	17.5	538.3	15.5	219.5	737.6	0.056551	0.0663915	0.21582E-03	0.0001579	
129	2.73	2.42E-37	296.0	18.0	538.3	16.0	219.5	737.6	0.056551	0.0663915	0.21582E-03	0.0001579	
130	2.73	2.42E-37	296.0	18.5	538.3	16.5	219.5	737.6	0.056551	0.0663915	0.21582E-03	0.0001579	
131	2.73	2.42E-37	296.0	19.0	538.3	17.0	219.5	737.6	0.056551	0.0663915	0.21582E-03	0.0001579	
132	2.73	2.42E-37	296.0	19.5	538.3	17.5	219.5	737.6	0.056551	0.0663915	0.21582E-03	0.0001579	
133	2.73	2.42E-37	296.0	20.0	538.3	18.0	219.5	737.6	0.056551	0.0663915	0.21582E-03	0.0001579	
134	2.73	2.42E-37	296.0	20.5	538.3	18.5	219.5	737.6	0.056551	0.0663915	0.21582E-03	0.0001579	
135	2.73	2.42E-37	296.0	21.0	538.3	19.0	219.5	737.6	0.056551	0.0663915	0.21582E-03	0.0001579	
136	2.73	2.42E-37	296.0	21.5	538.3	19.5	219.5	737.6	0.056551	0.0663915	0.21582E-03	0.0001579	
137	2.73	2.42E-37	296.0	22.0	538.3	20.0	219.5	737.6	0.056551	0.0663915	0.21582E-03	0.0001579	
138	2.73	2.42E-37	296.0	22.5	538.3	20.5	219.5	737.6	0.056551	0.0663915	0.21582E-03	0.0001579	
139	2.73	2.42E-37	296.0	23.0	538.3	21.0	219.5	737.6	0.056551	0.0663915	0.21582E-03	0.0001579	
140	2.73	2.42E-37	296.0	23.5	538.3	21.5	219.5	737.6	0.056551	0.0663915	0.21582E-03	0.0001579	
141	2.73	2.42E-37	296.0	24.0	538.3	22.0	219.5	737.6	0.056551	0.0663915	0.21582E-03	0.0001579	
142	2.73	2.42E-37	296.0	24.5	538.3	22.5	219.5	737.6	0.056551	0.0663915	0.21582E-03	0.0001579	
143	2.73	2.42E-37	296.0	25.0	538.3	23.0	219.5	737.6	0.056551	0.0663915	0.21582E-03	0.0001579	
144	2.73	2.42E-37	296.0	25.5	538.3	23.5	219.5	737.6	0.056551	0.0663915	0.21582E-03	0.0001579	
145	2.73	2.42E-37	296.0	26.0	538.3	24.0	219.5	737.6	0.056551	0.0663915	0.21582E-03	0.0001579	
146	2.73	2.42E-37	296.0	26.5	538.3	24.5	219.5	737.6	0.056551	0.0663915	0.21582E-03	0.0001579	
147	2.73	2.42E-37	296.0	27.0	538.3	25.0	219.5	737.6	0.056551	0.0663915	0.21582E-03	0.0001579	
148	2.73	2.42E-37	296.0	27.5	538.3	25.5	219.5	737.6	0.056551	0.0663915	0.21582E-03	0.0001579	
149	2.73	2.42E-37	296.0	28.0	538.3	26.0	219.5	737.6	0.056551				

POINT NO.	MINF	R芬T	QINF	X	DELTAP	PINF	UE	RHCM	RHCE	NUE	NUW	THETA	CF
117	3.89	2.42E 07	605.3	8.5	208.1	1350.0	928.0	C. C48418	C. C533208	0.25418E-03	0.21380E-03	0.0001623	0.0000700
118	3.93	2.51E 07	761.3	4.5	416.2	1695.0	837.2	0.660800	0.0666866	0.20315E-03	0.17121E-03	0.001061	C.030863
119	3.92	2.52E 07	761.0	5.0	354.5	1695.0	537.7	C. C6C145	C. C66E45	0.20329E-03	0.17125E-03	0.0001118	0.0000814
120	3.93	2.52E 07	761.0	5.5	373.5	1699.0	838.0	0.660737	0.0666827	0.20340E-03	0.17128E-03	0.0001171	0.0000776
121	3.93	2.52E 07	761.0	6.0	355.0	1695.0	838.4	0.660710	0.0666639	0.20350E-03	0.17131E-03	0.0001223	0.0000744
122	3.89	2.52E 07	761.0	6.5	336.4	1659.0	828.8	0.660691	0.0666752	0.20356E-03	0.17134E-03	0.0001273	0.0000714
123	3.92	2.32E 07	453.7	8.2	159.6	1211.0	837.3	0.036300	0.035973	0.338735E-03	0.28485E-03	0.0001821	0.0000832
124	3.89	2.32E 07	453.2	8.5	106.5	1211.0	837.6	0.036285	C. C35565	0.33885E-03	0.28489E-03	0.0001875	C.0000808
125	3.92	2.32E 07	453.0	9.0	105.5	1211.0	837.8	0.036262	C. C35557	0.33887E-03	0.28492E-03	0.0001929	0.0000786
126	3.92	2.32E 07	453.0	9.5	102.6	1211.0	838.1	0.036276	0.038949	0.33891E-03	0.28496E-03	0.0001982	C.0000764
127	3.93	2.32E 07	453.0	10.0	99.6	1211.0	838.4	0.036265	C. C35541	0.33902E-03	0.28501E-03	0.0002035	0.0000744
128	3.89	2.32E 07	453.0	10.5	96.5	1211.0	838.6	0.036259	0.039934	0.33906E-03	0.28504E-03	0.0002084	0.0000728
129	3.92	2.32E 07	492.0	8.5	134.3	867.0	927.6	0.313438	C.035437	0.39366E-03	0.31507E-03	0.0001871	C.0000826
130	3.99	2.32E 07	492.0	9.0	132.6	867.0	927.9	0.031427	0.035425	0.39078E-03	0.31512E-03	0.0001925	0.0000784
131	3.90	2.32E 07	492.0	9.5	131.2	867.0	928.2	0.031415	0.035420	0.29095E-03	0.31518E-03	0.0001975	C.0000762
132	3.92	2.32E 07	492.0	10.0	125.7	867.0	928.5	0.031406	0.035411	0.39103E-03	0.31522E-03	0.0002032	C.0000742
133	3.93	2.32E 07	492.0	10.5	128.2	867.0	928.8	0.031400	0.035404	0.39106E-03	0.31527E-03	0.0002078	0.0000724
134	3.90	2.32E 07	492.0	11.0	128.3	867.0	929.0	0.035397	0.39120E-03	0.31532E-03	0.0002127	0.0000708	
135	3.92	2.32E 07	492.0	11.5	128.3	867.0	929.3	0.031362	0.035386	0.39132E-03	0.31537E-03	0.0002175	0.0000702
136	3.93	2.32E 07	492.0	12.0	125.7	867.0	929.6	0.032921	0.035565	0.23565E-03	0.19366E-03	0.0001115	C.0000812
137	3.92	2.32E 07	492.0	12.5	127.5	867.0	930.0	0.035932	0.23585F-03	0.19371E-03	0.0001166	0.0000774	
138	3.93	2.32E 07	492.0	13.0	128.3	867.0	930.4	0.059522	0.059532	0.23600E-03	0.19075E-03	0.0001219	0.0000742
139	3.90	2.32E 07	492.0	13.5	128.3	867.0	930.7	0.059492	0.23607E-03	0.19375E-03	0.0001269	0.0000712	
140	3.95	2.42E 07	691.0	4.0	345.0	529.0	915.0	0.035660	0.045595	0.31274E-03	0.24839E-03	0.0001115	C.001016
141	3.95	2.42E 07	691.0	4.5	340.7	691.0	917.0	0.035671	C. C45C75	0.31313E-03	0.24837E-03	0.0001184	0.0000956
142	3.95	2.42E 07	691.0	5.0	322.2	1097.0	974.0	0.035684	0.039483	0.31353E-03	0.24844E-03	0.0001247	C.0000908
143	3.95	2.42E 07	691.0	5.5	305.1	1095.0	925.3	0.052555	0.059511	0.23600E-03	0.19075E-03	0.0001219	0.0000742
144	3.95	2.42E 07	691.0	6.0	335.0	1465.0	935.7	C. C522836	0.059492	0.23607E-03	0.19375E-03	0.0001269	0.0000712
145	3.95	2.42E 07	691.0	6.5	292.0	1297.0	975.6	0.039523	0.045024	0.31413E-03	0.24856E-03	0.0001305	0.0000866
146	3.95	2.42E 07	691.0	7.0	275.4	1097.0	977.4	0.035660	0.045595	0.31440E-03	0.24882E-03	0.0001362	0.0000828
147	3.95	2.42E 07	691.0	7.5	270.5	1097.0	977.4	0.035671	0.045595	0.31440E-03	0.24862E-03	0.0001420	C.0000794
148	3.95	2.42E 07	691.0	8.0	253.8	1097.0	977.1	0.035684	0.044981	0.31465E-03	0.24872E-03	0.0001525	C.0000740
149	3.95	2.42E 07	691.0	8.5	243.8	1097.0	977.4	0.035695	0.044969	0.31479E-03	0.24877E-03	0.0001571	C.0000718
150	3.95	2.52E 07	691.0	9.0	394.9	1382.0	977.0	0.039498	0.045595	0.31445E-03	0.24882E-03	0.0001619	C.0000896
151	3.95	2.52E 07	691.0	9.5	365.2	1382.0	977.0	0.039498	0.056415	0.25149F-03	0.19934E-03	0.0001115	C.0000810
152	3.95	2.52E 07	691.0	10.0	349.3	1382.0	978.7	0.049490	0.056374	0.25195E-03	0.19944E-03	0.0001168	0.0000774
153	3.95	2.52E 07	673.0	6.5	336.7	1382.0	979.1	0.049467	0.056356	0.25207E-03	0.19945E-03	0.0001267	C.0000712

ORIGINAL PAGE IS
OF POOR QUALITY

APPENDIX F
LISTING OF THE EXTENDED WU AND LOCK
PROGRAM WITH AN EXAMPLE RUN

ORIGINAL COPY IS
OF POOR QUALITY

```

C FIRST ITERATION :
C
C K515=.98
C
C NPI=NPI-1
C
C DO 4 I=2,12
C A=A+.01
C X(I)=93*.1-.21**3
C F(I)=98*.4+515*(I-1)+A*(C1*A+(C2+C3*A))
C Y(I)=A
C P1(I)=A
C CONTINUE
C
C 5 A=0.0
C H=X-L*C
C IT E=H-E+1
C
C 6 J=1,NPT
C A=-0.01
C Z=Z+A+H
C
C 7 CONTINUE
C
C 8 E13=F(I3)/SQR(1.0+Y(I3))-A1**2+X(I3)*DE/L/K515)**2)
C
C 9 I=2,NP1
C
C 10 CONTINUE
C
C 11 CALL SCK18(H,SE,Z,NPT)
C   FN11=0.0
C   FNK=Z(NPT)*GAMT*BE*F(I1)*SCTG*F(I1)
C   IF FNK.GT.0.0 IFN(I1)=FNK**THIRD
C   IF FN(I1).LT.0.0) FN(I1)=F(I1)*0.5
C   SF(I1)=FN(I1)-F(I1)
C   U(I1)=LBC-(FN(I1))*2/GAM
C   CONTINUE
C
C 12 CALL SCK18(H,FN,Z,NPT)
C   K515=1.0/Z(NPT)
C
C 13 DO 14 I=2,NPI
C   CALL SCK18(H,FN,Z,I1)
C   X(I1)=K515*Z(I1)
C   CONTINUE
C
C 14 DO 15 I=1,NPT
C   B:R=ABS(D(I1))
C

```

ORIGINAL DOCUMENT IS
OF POOR QUALITY


```

      CT(I)=FN(I)-F(I)
      U(I)=(Z-I*(V(I))-2)*2 /GAM
      CONTINUE
C
C     CALL SEKIB(H,FN,Z,RPT)
      KSIS=1./Z*NPT)
      00 0001200
      00 0001210
      00 0001220
C
      DO 80 I=2,NP1
      CALL SEKIB(H,FN,I,1)
      X(I)=KSIS*Z(I)
      CONTINUE
      00 0001230
      00 0001240
C
      ITER=ITER+1
      00 0001250
      00 0001260
      00 0001270
      00 0001280
      00 0001290
C
      DO 81 I=1,NP1
      F(I)=FN(I)
      CP(I)= -2.*U(I)-DEL**2*(1.-4.*((SIN(YETA))**2)*(SJ(NALFA))**2
      PTL=(I+5*GAMMA*CP(I))*MINF**2)/PT*GA2
      ZZ=PTL**(-1./GA2)-1.)*2./CA1
      ZZ=AMAX1(ZZ,ZERO)
      ZM(I)=SQRT(ZZ)
      CONTINUE
      00 0001300
      00 0001310
      00 0001320
      00 0001330
      00 0001340
      00 0001350
      00 0001360
      00 0001370
C
      IF(ITER>3)70,301,301
      201 CONTINUE
      MAX=0.0
      BAD=0.0
      00 0001380
      00 0001390
      00 0001400
      00 0001410
C
      DO 101 I=2,NP1
      IF(X(I)<-99)100,101,101
      BARF=ABS(D(I))
      C/F=CP(I)-CP(I-1)
      IF(C/F<=0.018AD=1.0
      MAX=AMAX1(MAX,BARF)
      CONTINUE
      00 0001420
      00 0001430
      00 0001440
      00 0001450
      00 0001460
      00 0001470
      00 0001480
      00 0001490
      00 0001500
      00 0001510
      00 0001520
      00 0001530
      00 0001540
C
      WRITE(16,26)ITER,KSIS
C
  103
  104
  105
  106
  107
  108
  109
  110
  111
  112
  113
  114
  115
  116
  117
  118
  119
  120
  121
  122
  123
  124
  125
  126
  127
  128
  129
  130
  131
  132
  133
  134
  135
  136
  137
  138
  139
  140
  141
  142
  143
  144
  145
  146
  147
  148
  149
  150
  151
  152
  153
  154
  155
  156
  157
  158
  159
  160
  161
  162
  163
  164
  165
  166
  167
  168
  169
  170
  171
  172
  173
  174
  175
  176
  177
  178
  179
  180
  181
  182
  183
  184
  185
  186
  187
  188
  189
  190
  191
  192
  193
  194
  195
  196
  197
  198
  199
  200
  201
  202
  203
  204
  205
  206
  207
  208
  209
  210
  211
  212
  213
  214
  215
  216
  217
  218
  219
  220
  221
  222
  223
  224
  225
  226
  227
  228
  229
  230
  231
  232
  233
  234
  235
  236
  237
  238
  239
  240
  241
  242
  243
  244
  245
  246
  247
  248
  249
  250
  251
  252
  253
  254
  255
  256
  257
  258
  259
  260
  261
  262
  263
  264
  265
  266
  267
  268
  269
  270
  271
  272
  273
  274
  275
  276
  277
  278
  279
  280
  281
  282
  283
  284
  285
  286
  287
  288
  289
  290
  291
  292
  293
  294
  295
  296
  297
  298
  299
  300
  301
  302
  303
  304
  305
  306
  307
  308
  309
  310
  311
  312
  313
  314
  315
  316
  317
  318
  319
  320
  321
  322
  323
  324
  325
  326
  327
  328
  329
  330
  331
  332
  333
  334
  335
  336
  337
  338
  339
  340
  341
  342
  343
  344
  345
  346
  347
  348
  349
  350
  351
  352
  353
  354
  355
  356
  357
  358
  359
  360
  361
  362
  363
  364
  365
  366
  367
  368
  369
  370
  371
  372
  373
  374
  375
  376
  377
  378
  379
  380
  381
  382
  383
  384
  385
  386
  387
  388
  389
  390
  391
  392
  393
  394
  395
  396
  397
  398
  399
  400
  401
  402
  403
  404
  405
  406
  407
  408
  409
  410
  411
  412
  413
  414
  415
  416
  417
  418
  419
  420
  421
  422
  423
  424
  425
  426
  427
  428
  429
  430
  431
  432
  433
  434
  435
  436
  437
  438
  439
  440
  441
  442
  443
  444
  445
  446
  447
  448
  449
  450
  451
  452
  453
  454
  455
  456
  457
  458
  459
  460
  461
  462
  463
  464
  465
  466
  467
  468
  469
  470
  471
  472
  473
  474
  475
  476
  477
  478
  479
  480
  481
  482
  483
  484
  485
  486
  487
  488
  489
  490
  491
  492
  493
  494
  495
  496
  497
  498
  499
  500
  501
  502
  503
  504
  505
  506
  507
  508
  509
  510
  511
  512
  513
  514
  515
  516
  517
  518
  519
  520
  521
  522
  523
  524
  525
  526
  527
  528
  529
  530
  531
  532
  533
  534
  535
  536
  537
  538
  539
  540
  541
  542
  543
  544
  545
  546
  547
  548
  549
  550
  551
  552
  553
  554
  555
  556
  557
  558
  559
  560
  561
  562
  563
  564
  565
  566
  567
  568
  569
  570
  571
  572
  573
  574
  575
  576
  577
  578
  579
  580
  581
  582
  583
  584
  585
  586
  587
  588
  589
  590
  591
  592
  593
  594
  595
  596
  597
  598
  599
  600
  601
  602
  603
  604
  605
  606
  607
  608
  609
  610
  611
  612
  613
  614
  615
  616
  617
  618
  619
  620
  621
  622
  623
  624
  625
  626
  627
  628
  629
  630
  631
  632
  633
  634
  635
  636
  637
  638
  639
  640
  641
  642
  643
  644
  645
  646
  647
  648
  649
  650
  651
  652
  653
  654
  655
  656
  657
  658
  659
  660
  661
  662
  663
  664
  665
  666
  667
  668
  669
  670
  671
  672
  673
  674
  675
  676
  677
  678
  679
  680
  681
  682
  683
  684
  685
  686
  687
  688
  689
  690
  691
  692
  693
  694
  695
  696
  697
  698
  699
  700
  701
  702
  703
  704
  705
  706
  707
  708
  709
  710
  711
  712
  713
  714
  715
  716
  717
  718
  719
  720
  721
  722
  723
  724
  725
  726
  727
  728
  729
  730
  731
  732
  733
  734
  735
  736
  737
  738
  739
  740
  741
  742
  743
  744
  745
  746
  747
  748
  749
  750
  751
  752
  753
  754
  755
  756
  757
  758
  759
  760
  761
  762
  763
  764
  765
  766
  767
  768
  769
  770
  771
  772
  773
  774
  775
  776
  777
  778
  779
  780
  781
  782
  783
  784
  785
  786
  787
  788
  789
  790
  791
  792
  793
  794
  795
  796
  797
  798
  799
  800
  801
  802
  803
  804
  805
  806
  807
  808
  809
  810
  811
  812
  813
  814
  815
  816
  817
  818
  819
  820
  821
  822
  823
  824
  825
  826
  827
  828
  829
  830
  831
  832
  833
  834
  835
  836
  837
  838
  839
  840
  841
  842
  843
  844
  845
  846
  847
  848
  849
  850
  851
  852
  853
  854
  855
  856
  857
  858
  859
  860
  861
  862
  863
  864
  865
  866
  867
  868
  869
  870
  871
  872
  873
  874
  875
  876
  877
  878
  879
  880
  881
  882
  883
  884
  885
  886
  887
  888
  889
  890
  891
  892
  893
  894
  895
  896
  897
  898
  899
  900
  901
  902
  903
  904
  905
  906
  907
  908
  909
  910
  911
  912
  913
  914
  915
  916
  917
  918
  919
  920
  921
  922
  923
  924
  925
  926
  927
  928
  929
  930
  931
  932
  933
  934
  935
  936
  937
  938
  939
  940
  941
  942
  943
  944
  945
  946
  947
  948
  949
  950
  951
  952
  953
  954
  955
  956
  957
  958
  959
  960
  961
  962
  963
  964
  965
  966
  967
  968
  969
  970
  971
  972
  973
  974
  975
  976
  977
  978
  979
  980
  981
  982
  983
  984
  985
  986
  987
  988
  989
  990
  991
  992
  993
  994
  995
  996
  997
  998
  999
  1000
  1001
  1002
  1003
  1004
  1005
  1006
  1007
  1008
  1009
  1010
  1011
  1012
  1013
  1014
  1015
  1016
  1017
  1018
  1019
  1020
  1021
  1022
  1023
  1024
  1025
  1026
  1027
  1028
  1029
  1030
  1031
  1032
  1033
  1034
  1035
  1036
  1037
  1038
  1039
  1040
  1041
  1042
  1043
  1044
  1045
  1046
  1047
  1048
  1049
  1050
  1051
  1052
  1053
  1054
  1055
  1056
  1057
  1058
  1059
  1060
  1061
  1062
  1063
  1064
  1065
  1066
  1067
  1068
  1069
  1070
  1071
  1072
  1073
  1074
  1075
  1076
  1077
  1078
  1079
  1080
  1081
  1082
  1083
  1084
  1085
  1086
  1087
  1088
  1089
  1090
  1091
  1092
  1093
  1094
  1095
  1096
  1097
  1098
  1099
  1100
  1101
  1102
  1103
  1104
  1105
  1106
  1107
  1108
  1109
  1110
  1111
  1112
  1113
  1114
  1115
  1116
  1117
  1118
  1119
  1120
  1121
  1122
  1123
  1124
  1125
  1126
  1127
  1128
  1129
  1130
  1131
  1132
  1133
  1134
  1135
  1136
  1137
  1138
  1139
  1140
  1141
  1142
  1143
  1144
  1145
  1146
  1147
  1148
  1149
  1150
  1151
  1152
  1153
  1154
  1155
  1156
  1157
  1158
  1159
  1160
  1161
  1162
  1163
  1164
  1165
  1166
  1167
  1168
  1169
  1170
  1171
  1172
  1173
  1174
  1175
  1176
  1177
  1178
  1179
  1180
  1181
  1182
  1183
  1184
  1185
  1186
  1187
  1188
  1189
  1190
  1191
  1192
  1193
  1194
  1195
  1196
  1197
  1198
  1199
  1200
  1201
  1202
  1203
  1204
  1205
  1206
  1207
  1208
  1209
  1210
  1211
  1212
  1213
  1214
  1215
  1216
  1217
  1218
  1219
  1220
  1221
  1222
  1223
  1224
  1225
  1226
  1227
  1228
  1229
  1230
  1231
  1232
  1233
  1234
  1235
  1236
  1237
  1238
  1239
  1240
  1241
  1242
  1243
  1244
  1245
  1246
  1247
  1248
  1249
  1250
  1251
  1252
  1253
  1254
  1255
  1256
  1257
  1258
  1259
  1260
  1261
  1262
  1263
  1264
  1265
  1266
  1267
  1268
  1269
  1270
  1271
  1272
  1273
  1274
  1275
  1276
  1277
  1278
  1279
  1280
  1281
  1282
  1283
  1284
  1285
  1286
  1287
  1288
  1289
  1290
  1291
  1292
  1293
  1294
  1295
  1296
  1297
  1298
  1299
  1300
  1301
  1302
  1303
  1304
  1305
  1306
  1307
  1308
  1309
  1310
  1311
  1312
  1313
  1314
  1315
  1316
  1317
  1318
  1319
  1320
  1321
  1322
  1323
  1324
  1325
  1326
  1327
  1328
  1329
  1330
  1331
  1332
  1333
  1334
  1335
  1336
  1337
  1338
  1339
  1340
  1341
  1342
  1343
  1344
  1345
  1346
  1347
  1348
  1349
  1350
  1351
  1352
  1353
  1354
  1355
  1356
  1357
  1358
  1359
  1360
  1361
  1362
  1363
  1364
  1365
  1366
  1367
  1368
  1369
  1370
  1371
  1372
  1373
  1374
  1375
  1376
  1377
  1378
  1379
  1380
  1381
  1382
  1383
  1384
  1385
  1386
  1387
  1388
  1389
  1390
  1391
  1392
  1393
  1394
  1395
  1396
  1397
  1398
  1399
  1400
  1401
  1402
  1403
  1404
  1405
  1406
  1407
  1408
  1409
  1410
  1411
  1412
  1413
  1414
  1415
  1416
  1417
  1418
  1419
  1420
  1421
  1422
  1423
  1424
  1425
  1426
  1427
  1428
  1429
  1430
  1431
  1432
  1433
  1434
  1435
  1436
  1437
  1438
  1439
  1440
  1441
  1442
  1443
  1444
  1445
  1446
  1447
  1448
  1449
  1450
  1451
  1452
  1453
  1454
  1455
  1456
  1457
  1458
  1459
  1460
  1461
  1462
  1463
  1464
  1465
  1466
  1467
  1468
  1469
  1470
  1471
  1472
  1473
  1474
  1475
  1476
  1477
  1478
  1479
  1480
  1481
  1482
  1483
  1484
  1485
  1486
  1487
  1488
  1489
  1490
  1491
  1492
  1493
  1494
  1495
  1496
  1497
  1498
  1499
  1500
  1501
  1502
  1503
  1504
  1505
  1506
  1507
  1508
  1509
  1510
  1511
  1512
  1513
  1514
  1515
  1516
  1517
  1518
  1519
  1520
  1521
  1522
  1523
  1524
  1525
  1526
  1527
  1528
  1529
  1530
  1531
  1532
  1533
  1534
  1535
  1536
  1537
  1538
  1539
  1540
  1541
  1542
  1543
  1544
  1545
  1546
  1547
  1548
  1549
  1550
  1551
  1552
  1553
  1554
  1555
  1556
  1557
  1558
  1559
  1560
  1561
  1562
  1563
  1564
  1565
  1566
  1567
  1568
  1569
  1570
  1571
  1572
  1573
  1574
  1575
  1576
  1577
  1578
  1579
  1580
  1581
  1582
  1583
  1584
  1585
  1586
  1587
  1588
  1589
  1590
  1591
  1592
  1593
  1594
  1595
  1596
  1597
  1598
  1599
  1600
  1601
  1602
  1603
  1604
  1605
  1606
  1607
  1608
  1609
  1610
  1611
  1612
  1613
  1614
  1615
  1616
  1617
  1618
  1619
  1620
  1621
  1622
  1623
  1624
  1625
  1626
  1627
  1628
  1629
  1630
  1631
  1632
  1633
  1634
  1635
  1636
  1637
  1638
  1639
  1640
  1641
  1642
  1643
  1644
  1645
  1646
  1647
```

```

111 IF(IALFA .LE. 310, 311, 310
112 EO 300 I=1,NPT
113 CD(I,I)=CP(I,I)*X(I,I)*KSIS*FN(I,I)
114 CONTINUE
115 CALL SEKISI(W,CD(i,Z,NPT)
116 CD=2.*Z(NPT)

117 WRITE(6,801)CD
118 CONTINUE
119 C
120 GCN4=.5*GAMMA*HINF**2
121 HUNKY=.5*TAN(IDEAL)
122 WRITE(6,227)
123 DO 92 K=1,NPT
124 D=X(K)*HUNKY
125 PI(K)=CP(K)*GCN4+1.0
126 WRITE(6,228) K,X(K),CP(K),Z4(K),P(K),K
127 CONTINUE
128
129 C
130 FORMAT(//10X,'ANGLE OF ATTACK=',F10.3,5X,'ANGLE OF YAW=',F10.3,
131 2'DEGREES')/
132 FORMAT(//10X,'SUPERSONIC FLOW = NO CONVERGENCE '///)
133 FORMAT(//20X,12,' ITERATIONS ',5X,'KSAT(SONIC) * ',F15.5/)
134 FORMAT(//25X,'X/L' 'T41,'CP' ,T57,'M' ,Y70,'P/PINF' /)
135 FORMAT(115,4F15.5,11G)
136 FORMAT(//20X,' MACH INF = ',F8.4,5X,'CONE SEMI-VERTEX ANGLE = '
137 'F9.6,'1DEG10.'5X,'GAMMA = ',F8.3/)
138 FORMAT(//10X,' DRAG COEFFICIENT = ',F13.5//)
139 IF (IPASS.EQ.2) GOTO 96
140 READ (5,301)P2
141 CALL DISI (4INF,REFT,QINFI)
142 IF (IPASS.EQ.1) GO TO 95
143 CALL INITIA
144 WRITE (7,95)
145 FORMAT(90*'')
146 WRITE(6,94)
147 FORMAT(1H1)
148 GO TO 36
149 STOP
150 END

```

ORIGINAL PAGE IS
OF POOR QUALITY

```
C
C      SUBROUTINE SEKIB
C      ****
C
C      SUBROUTINE SEKIB(H,W,Z,NDIM)
C      DIMENSION H(1125),W(1125)
C      SUM2=0.0
C      DO 1 I=2,NDIM
C      SUM1=0.0
C      SUM2=SUM2+H(I)*W(I)+W(I-1)
C      1   Z(I-1)=SUM1
C      Z(NDIM)=SUM2
C
C      RETURN
C
C      END
```

```

C C SUBROUTINE ANGLES
C *****
C THIS SUBPROGRAM CALCULATES THE EFFECTIVE ANGLE OF ATTACK AND THE
C AZIMUTH ANGLE OF THE FLOW NEEDED IN THE MAIN PROGRAM.
C
C SUBROUTINE ANGLES(ALFA,BETA,THETA)
C
C DOUBLE PRECISION DALFA,DALFAB,DBETA,DTHETA,X,Y,Z,RAD
C
RAD=57.2957800
IF (BETA .NE. 0.0) GO TO 2
IF (ALFA .LT. 0.0 ) GO TO 5
THETA=0.0
GO TO 4
5   THETA = 180.0
GO TO 4
C
C DALFA=ALFA/RAD
CDBETA=BETAV/RAD
Y=DCOS(DBETA)*DTAN(DALFA)
DTHTETA=DATAN(Y)
X=DCOS(DBETA)*DCOS(DTHETA)
DALFAB=DARCSIN(X)
Z=Y/DTAN(DALFAB)
DTHETA=DARCSIN(Z)
ALFA3=DALFAB*RAD
C
C ALFA3 = EFFECTIVE ANGLE OF ATTACK.
C
THETA=DTHETA*RAD
IF (ALFA .LT. 0.0 ) DALFAB=-ALFAB
IF (BETA .LT. 0.0 ) THETA=-THE TA
ALFA=ALFA3
CONTINUE
4
C
C WRITE(6,1) DALFA,THETA
1 FORMAT(1X,'EFFECTIVE ANGLE OF ATTACK =',F9.3,' DEGREES',
      $ '1X,'AZIMUTH ANGLE =',F9.3,' DEGREES',/)
RETURN
END

```

```

C
C   SUBROUTINE DIST
C
C   THIS SUBPROGRAM CALCULATES THE FREE-STREAP CONDITIONS AS WELL AS
C   THE VELOCITY DISTRIBUTION AT THE EDGE OF THE ECLIPSY LAYER TO BE
C   USED AS BOUNDARY CONDITIONS TO A BOUNDARY LAYER SOLVING PROGRAM.
C
C   SUBROUTINE DIST (IINF,REFT,CINF)
C
C   DIMENSION T(125)
C
C   COMMON /MSRA/ PT, GAMMA, GA1, GA2, GCHN
C   COMMON /SUE/ FTCT, PI125, V125, X125, ZM125
C
C   COMMON /JINF/ PINF, TINF, VINF
C   COMMON /PARM/ NPT, ISTART, XL, IPASS, DELTA
C
C   ZM'S = LOCAL MACH NUMBERS.
C
C   REAL PINF, MUINF
C
C   MUINF = FREE-STREAM DYNAMIC VISCOSITY LBF S/F 10-2.
C
C   E=1.7573E+06
C   C=3.5654E+08
C   A=REFT*MINF/CINF
C   CNST=Gamma*1.716*C
C   FTCT=CINF*PT*GA2/CCPM
C
C   FTCT = FREE-STREAM TOTAL PRESSURE PSF.
C
C   IINF=(R+SORT10+4.0*A*C)/2.0/A
C   TICT=TINF*PT
C
C   IINF = FREE-STREAM STATIC TEMPERATURE RANKIN.
C   TICT = TOTAL TEMPERATURE.
C
C   MUINF=2.27E-08*IINF*SQRT(IINF)/(IINF+158.6)
C   VINF=SCRT(CCST*TINF)*PINF
C   PINF=PTOT/PT+GA2
C   F=CINF*PINF/52.35/TINF
C
C

```

ORIGIN OF POOR QUALITY

```

00002520
00002530
00002540
00002550
00002560
00002570

1C3      WRITE(6,100) PINF,TINF,VINF,RHINF,MUINF
        FCAPAT(5X,G13.4)
        EC 1C 1=1,NPT
        T(1)=T00/(1.0+J-5*(AI)*(M(1)**2))
        V(1)=Z(1)*SCRIT(CAST*T(1))

C      T*S = LOCAL STATIC TEMPERATURES F1/S.
C      V*S = EDGE VELOCITIES F1/S.

10       CCAT INUE
        WRITE(6,93)
        FFORMAT(//45X,'VELOCITY DISTRIBUTION : /')
        WRITE(6,250)
        FFORMAT(// 5IX,'V' ,13X,'X/L' ,13X,'U' /)
        WRITE(6,200) I,J,ZM(I,J),V(I,J),I=1,NP1)
        FCAPAT(5X,15.5X,F10.5,5X,F10.5,5X,F10.2 )
        FEI FN

13       WRITE(6,300)
        FFORMAT(5X,'MAX. ITERATIONS EXCEEDED: /')
        RETURN
        END

C      VINF = FREE-STREAM VELOCITY.
C      R+CINF = FREE-STREAM DENSITY 1BM/F1**3.
C      PINF = FREE-STREAM STATIC PRESSURE PSF.

150      TCT=TINF/APT
        WRITE(6,150)
        FFORMAT(//7X,'MINF',12X,'RE/FT',11X,'QINF /')
        WRITE(6,110) MINF,REFT,QINF
        FFORMAT(3(5X,G10.4))
        WRITE(6,160)
        FFORMAT(//5X,'PICTAL',9X,'TTCTAL',/)

160      WRITE(6,120) PICT,T1Q1
        FFORMAT(2(5X,G10.4))
        WRITE(6,170)
        FFORMAT(//6X,'PINF',11X,'TINF',11X,'UINF',12X,'RHINF',10X,'MUINF')
        FFORMAT(//6X,'PINF',11X,'TINF',11X,'UINF',12X,'RHINF',10X,'MUINF')

```

```

C
C SUBROUTINE INITIA
*****
C THIS SUBPROGRAM CALCULATES INITIAL VELOCITY AND TOTAL ENTHALPY
C PROFILES IN THE BOUNDARY LAYER NEAR THE TIP OF THE CONE WHICH IS
C NEEDED IN STAN-5 PROGRAM.
C
C SUBROUTINE INITIA
COMMON /SUB/ PTOI,P(125),V(125),X(125),ZM(125)
COMMON /INIF/ PINF,TINF,VINF
COMMON /PARM/ NPT,ISTART,T,MAXIT,TCL,TTOT,XL,IPASS,DELTA
DIMENSION ETA(30),PRIME(30),RM(125)
REAL MIN,MUSTAR,NUSTAR
DATA PR/0.77/
DATA ZM/0.77/
C
C BLASIUS SOLUTION.
C
C DATA ETA/0.0,0.1,0.2,0.3,0.4,0.5,0.6,0.7,C,8,C,9,1,0,I,1,1,2,1,3,
      51.4,1.5,1.6,1.7,1.8,1.9,2.0,2.2,2.4,2.6,2.8,3.0,3.4,3.8,4.2,5.0/
C DATA PRIME/0.0,0.04656,0.09391,0.14081,C.18761,C.23423,0.28058,
      52.32653,0.37196,0.41672,0.46063,0.50354,0.54525,0.58559,0.62439,
      53.66147,0.59670,0.72593,0.76106,0.79000,0.81669,0.86330,0.90107,
      54.93060,0.95288,0.96505,0.98757,0.99594,C.98822,1.0/
C
C READ 15,PR XLE
      READ 15,PR
      XLE=PR/12.0/XL
      XLE=0
      DYLE=0
      IF ( XLE.LT.X(1) ) GO TO 57
      DO 61 I=1,NPT
      IF ( XLE.EQ.X(I) ) OR ( XLE.GT.X(I) ) AND ( XLE.LT.X(I+1) ) GO TO 64
      61 CONTINUE
      IF ( XLE.EQ.0 ) GO TO 67
      64
      XIN=X(ISTART)*XL
      MIN=ZM(ISTART)
      UE=V(ISTART)
      R=SQRTPR
      C
      C R = RECOVERY FACTOR, PR = PRANDTL NUMBER.
      C

```

```

I=1,IJ/I(1,3+0,2*MIN**2)          00 002 820
I=1,I*(1,3+R*3,2*MIN**2)          CO C02 830

C   TW = WALL TEMPERATURE = ADIABATIC WALL TEMPERATURE APPROXIMATELY.

C   TSTAR=T*(3.5+0.039*I*MIN**2+0.5*TWT)
      MUSTAR=2.27E-08*TSTAR*SQR(TSTAR)/ITSTAR+198.6)    00 002 840
      00 002 855

C   THESE ARE THE AVERAGE TEMPERATURE AND DYNAMIC VISCOSITY ACROSS
C   THE BOUNDARY LAYER AT THE INITIAL LOCATION.

C   PIN=PI*ISTART*T*PINF           00 002 860

C   INITIAL STATIC PRESSURE.

C   WRITE(6,90)
      90  FORMAT(3X,'TW',10X,'PINIT',/)
      WRITE(6,90) TW,PIN
      FORMAT(5X,F8.2,6X,F8.2//)
      80  WRITE(7,70) PIN
      FORMAT(F10.2)
      CC 60 I=ISTART,IXLE
      AI(I)=XL
      K(I)=X(I)*SINIDELTA/ST.29578}
      C
      Rn'S ARE THE RADII OF THE CONE SURFACE AT THE VARIOUS X'S.

C   WRITE(7,50) X(I),RW(I)
      50  FORMAT(2(SX,F10.6))
      CONTINUE
      60  DO 40 I=ISTART,IXLE
          WRITE(E(7,30),V(I))
          FORMAT(5X,F10.2)
      40  C
      THE EDGE VELOCITIES.

C   COUNTINUE
      40  ROSTAR=PIN/S3/TSTAR
      MUSTAR=MUSTAR/RNSTAR*32.174
      YFACT=SQR(1.3-0.0*UE/2.0/NUSTAR/XIN)
      HFACT=5.075*6/(1.0-R)
      HIN=3.24*TW
      WRITE(6,100)
      FORMAT(10I,10X,'Y',16X,'U',14X,'H//')
      100  DO 20 I=1,30
      20  C

```

```

Y=ETAL1/YFACT
U=UE*FPRI*E11
H=HIN+UE*2/HFACT
C
C      Y = THE NORMAL DISTANCE FROM CONE SURFACE IN FEET, U & H ARE THE
C      VELOCITY AND STAGNATION ENTHALPY PROFILES RESPECTIVELY.
C
C      WRITE(6,10) Y,U,H
C      WRITE(7,10) Y,U,H
C      FORMAT(5X, E10.4,2(5X,F10.2))
10     CONTINUE
20     RETURN
67     WRITE(6,69) XLE
69     FORMAT(5X, 'ERROR IN XLE. VALUE READ =',2X,FB .5)
      RETURN
END

```

21	0.23636	0.04341	0.48853	1.00760
22	0.21448	0.04263	0.48868	1.00749
23	0.22460	0.04226	0.48883	1.00739
24	0.23471	0.04170	0.48898	1.00730
25	0.24483	0.04116	0.48913	1.00720
26	0.25496	0.04062	0.48927	1.00711
27	0.26505	0.04009	0.48941	1.00701
28	0.27517	0.03556	0.48955	1.00652
29	0.28528	0.03904	0.48969	1.00683
30	0.29539	0.03853	0.48982	1.00674
31	0.30549	0.03801	0.48996	1.00665
32	0.31560	0.03750	0.49009	1.00656
33	0.32571	0.03700	0.49021	1.00647
34	0.33581	0.03649	0.49037	1.00638
35	0.34592	0.03598	0.49050	1.00630
36	0.35602	0.03547	0.49063	1.00621
37	0.36612	0.03497	0.49077	1.00612
38	0.37622	0.03446	0.49091	1.00603
39	0.38632	0.03394	0.49104	1.00594
40	0.39642	0.03343	0.49118	1.00585
41	0.40652	0.03291	0.49131	1.00576
42	0.41662	0.03238	0.49145	1.00567
43	0.42671	0.03186	0.49160	1.00557
44	0.43681	0.03132	0.49174	1.00548
45	0.44690	0.03078	0.49188	1.00539
46	0.45700	0.03024	0.49202	1.00529
47	0.46709	0.02968	0.49217	1.00515
48	0.47718	0.02912	0.49232	1.00510
49	0.48727	0.02855	0.49247	1.00500
50	0.49736	0.02796	0.49263	1.00489
51	0.50744	0.02737	0.49278	1.00479
52	0.51753	0.02676	0.49294	1.00468
53	0.52761	0.02615	0.49311	1.00457
54	0.53770	0.02551	0.49328	1.00446
55	0.54778	0.02487	0.49344	1.00435
56	0.55786	0.02420	0.49362	1.00424
57	0.56794	0.02352	0.49380	1.00412
58	0.57802	0.02282	0.49399	1.00399
59	0.58809	0.02210	0.49418	1.00387
60	0.59817	0.02136	0.49437	1.00374
61	0.60824	0.02059	0.49457	1.00360
62	0.61832	0.01980	0.49476	1.00346
63	0.62839	0.01898	0.49500	1.00332
64	0.63846	0.01913	0.49522	1.00317
65	0.64852	0.01725	0.49546	1.00302
66	0.65859	0.01633	0.49570	1.00286

67	0.65865	0.31537	0.49595	1.00269	67
69	0.67071	0.01437	0.49622	1.00251	68
69	0.63877	0.01332	0.49649	1.00233	69
70	0.65893	0.01223	0.49678	1.00214	70
71	0.717839	0.01107	0.49708	1.00194	71
72	0.71894	0.00996	0.49741	1.00172	72
73	0.72699	0.00857	0.49775	1.00150	73
74	0.73954	0.00721	0.49810	1.00126	74
75	0.74938	0.00576	0.49848	1.00101	75
76	0.75912	0.00422	0.49889	1.00074	76
77	0.76916	0.00259	0.49932	1.00045	77
78	0.77920	0.00281	0.49979	1.00014	78
79	0.78923	-0.00109	0.50028	0.99581	79
80	0.79926	-0.00315	0.50082	0.9945	80
81	0.80928	-0.00538	0.50141	0.99516	81
82	0.81930	-0.00782	0.50205	0.99863	82
83	0.82931	-0.01050	0.50275	0.99816	83
84	0.83932	-0.01345	0.50352	0.99765	84
85	0.84932	-0.01674	0.50438	0.99707	85
85	0.85932	-0.02042	0.50534	0.99643	86
87	0.86931	-0.02459	0.50643	0.99570	87
88	0.87928	-0.02934	0.50766	0.99497	88
89	0.88925	-0.03482	0.50909	0.99391	89
90	0.89921	-0.04124	0.51076	0.99278	90
91	0.90915	-0.04886	0.51273	0.99145	91
92	0.91907	-0.05810	0.51512	0.98953	92
93	0.92898	-0.06955	0.51807	0.98783	93
94	0.93835	-0.08416	0.52162	0.98527	94
95	0.94870	-0.10352	0.52677	0.98168	95
96	0.95849	-0.13054	0.53364	0.97716	96
97	0.96822	-0.17107	0.54386	0.9706	97
98	0.97703	-0.23915	0.56082	0.95815	98
99	0.98722	-0.37904	0.59455	0.93367	99
100	0.99592	-0.84974	0.70507	0.85130	100
101	1.00000	-2.5C762	1.09189	0.56117	101

W_{INF}	q_E/FT	Q_{INF}
-500.0	-4000E+37	404.0
P_{TAL}	T_{TAL}	U_{TAL}
273.0	530.8	
P_{INF}	T_{INF}	U_{INF}
230.0	505.5	551.1
		-85559 E-01
		-3666 E-06

VELOCITY DISTRIBUTION :

	x/l	u
1	0.0	0.0
2	0.48140	0.01181
3	0.48255	0.02197
4	0.48389	0.03213
5	0.48452	0.04228
6	0.48522	0.05242
7	0.48543	0.06257
8	0.48578	0.07271
9	0.48605	0.08284
10	0.48637	0.09298
11	0.48663	0.10311
12	0.48687	0.11325
13	0.48709	0.12338
14	0.48730	0.13350
15	0.48749	0.14362
16	0.48769	0.15376
17	0.48787	0.16388
18	0.48804	0.17400
		5.38E-45

LAST PAGE IS
OF POOR QUALITY

19	0.48820	0.18412	538.62
20	0.48831	0.15424	538.80
21	0.48853	0.20436	538.96
22	0.48868	0.21449	539.13
23	0.48883	0.22460	539.29
24	0.48898	0.23471	539.44
25	0.48913	0.24483	539.60
26	0.48927	0.25494	539.74
27	0.48941	0.26505	539.89
28	0.48955	0.27517	540.04
29	0.48969	0.28526	540.19
30	0.48982	0.29539	540.33
31	0.48996	0.30549	540.47
32	0.49009	0.31560	540.62
33	0.49023	0.32571	540.76
34	0.49037	0.33581	540.90
35	0.49050	0.34592	541.04
36	0.49063	0.35602	541.18
37	0.49077	0.36612	541.33
38	0.49091	0.37622	541.47
39	0.49104	0.38632	541.61
40	0.49118	0.39642	541.76
41	0.49131	0.40652	541.90
42	0.49145	0.41662	542.05
43	0.49160	0.42671	542.20
44	0.49174	0.43681	542.34
45	0.49188	0.44690	542.49
46	0.49202	0.45700	542.64
47	0.49217	0.46709	542.80
48	0.49232	0.47718	542.95
49	0.49247	0.48727	543.12
50	0.49263	0.49736	543.28
51	0.49278	0.50744	543.44
52	0.49294	0.51753	543.61
53	0.49311	0.52761	543.78
54	0.49328	0.53770	543.96
55	0.49344	0.54778	544.14
56	0.49362	0.55786	544.32
57	0.49380	0.56794	544.52
58	0.49395	0.57602	544.71
59	0.49418	0.58809	544.91
60	0.49437	0.59817	545.11
61	0.49457	0.60824	545.33
62	0.49479	0.61832	545.55
63	0.49500	0.62835	545.77
64	0.49522	0.63846	546.01

65	0.49546	0.64852
66	0.49570	0.65655
67	0.49595	0.66655
68	0.49622	0.67671
69	0.49649	0.68977
70	0.49678	0.69883
71	0.49708	0.7089
72	0.49741	0.71094
73	0.49775	0.72695
74	0.49810	0.73504
75	0.49848	0.74608
76	0.49885	0.75512
77	0.49932	0.76916
78	0.49979	0.77920
79	0.50028	0.78623
80	0.50082	0.79926
81	0.50141	0.80925
82	0.50205	0.81530
83	0.50275	0.82931
84	0.50342	0.83632
85	0.50438	0.84532
86	0.50534	0.85932
87	0.50642	0.86631
88	0.50766	0.87928
89	0.50909	0.88625
90	0.51076	0.89521
91	0.51273	0.90915
92	0.51512	0.91607
93	0.51807	0.92898
94	0.52182	0.93885
95	0.52677	0.94870
96	0.53364	0.95849
97	0.54386	0.96222
98	0.56082	0.97783
99	0.59495	0.98722
100	0.70507	0.99592
101	1.09185	1.00000

T _w	P INIT	V	U	H
527.24	2334.45	0.0	126.54	
		25.34	126.54	
		50.07	126.54	
		75.37	126.55	
		100.32	126.57	
		124.87	126.58	
		149.59	126.60	
		174.06	126.63	
		199.30	126.66	
		222.17	126.69	
		245.58	126.72	
		268.45	126.76	
		293.69	126.79	
		312.20	126.83	
		332.88	126.87	
		352.65	126.91	
		371.43	126.95	
		399.15	127.00	
		405.74	127.04	
		421.17	127.07	
		435.40	127.11	
		460.25	127.16	
		480.39	127.24	
		495.13	127.28	
		508.01	127.32	
		516.63	127.34	
		526.72	127.38	
		530.97	127.39	
		532.50	127.39	
		533.13	127.40	

ORIGINAL PAGE IS
OF POOR QUALITY.